J Mater Sci (2012) 47:1–22
DOI 10.1007/s10853-011-5865-1

ANNIVERSARY REVIEW

Probing material properties with sharp indenters: a retrospective

Brian R. Lawn · Robert F. Cook

Received: 1 July 2011 / Accepted: 8 August 2011 / Published online: 31 August 2011

Abstract A retrospective on the use of sharp, fixed-profile indenters as materials probes is presented. Indentation is proposed as a simple but powerful methodology for evaluating basic mechanical properties—elastic modulus, hardness, toughness—in all classes of materials. Indentation also provides unique insight into fundamental deformation and fracture processes. Of particular interest is the existence of intrinsic size effects as characteristic contact dimensions pass from macro- to micro- to nano-scale dimensions. The utility of indentations as 'controlled flaws' in the context of strength of materials is outlined. The roles of two other important material factors—rate effects and microstructure—are considered. Examples of technological and biological applications are presented as illustrations of the widespread power of the technique. Strengths and limitations of the methodology as a routine testing protocol are discussed.

Introduction

The use of indentations to probe the properties of materials extends back several centuries [1–4]. The most common indenters are made of ultra-hard materials, such as diamond or tungsten carbide, in order to produce well-formed impressions in test specimens without themselves suffering damage. Their geometry is usually one of two kinds: 'sharp' with a fixed profile—pyramidal with four sides (Vickers, Knoop) or three sides (Berkovich, cube corner)—or conical; 'blunt' with a characteristic radius of curvature, i.e. spherical (Hertzian). Our focus in this article will be on fixed-profile indenters, building on earlier review articles [5–7]. Those readers specifically interested in Hertzian indentation are referred elsewhere [5, 8, 9]. Indentation stress fields may be usefully described in terms of characteristic scaling quantities: the *spatial* extent of the field by some characteristic impression size; the *intensity* of the field by contact pressure. Analysis of sharp indenter behaviour is simplified by a certain 'geometrical similarity' in the stress fields, insofar as the contact pressure remains independent of size [2, 5]. Contacts with fixed-profile indenters are largely elastic–plastic [10], with the balance between competing deformation modes dependent on material type: in metals, more plastic, with relatively little impression recovery; in ceramics, more elastic, with substantial recovery and accompanying fracture; in polymers, viscoelastic, with partial recovery; in composites, all of the above. The stresses beneath sharp indenters are uncharacteristically intense, in some materials approaching the cohesive strength of the specimen material, often providing the only practical means of sampling point-to-point intrinsic structural properties.

Indentations may be considered as 'fingerprints' containing vital information about the mechanical response of a given material. Select illustrative examples are shown in Fig. 1, for a range of material types and contact sizes. Quite apart from its diagnostic potential, indentation provides the means for routine quantitative measurement of material properties: the size of a well-formed indentation is a measure of hardness; the degree to which any such impression 'recovers' on unloading is a measure of elastic modulus; the time dependence of the loading–unloading cycle measures 'loss' (as opposed to 'storage') modulus; and the size of attendant cracks at the impression corners measures toughness. We are interested in all these

B. R. Lawn (✉) · R. F. Cook
Ceramics Division, National Institute of Standards and Technology, Gaithersburg, MD 20899, USA
e-mail: brianlawn@gmail.com

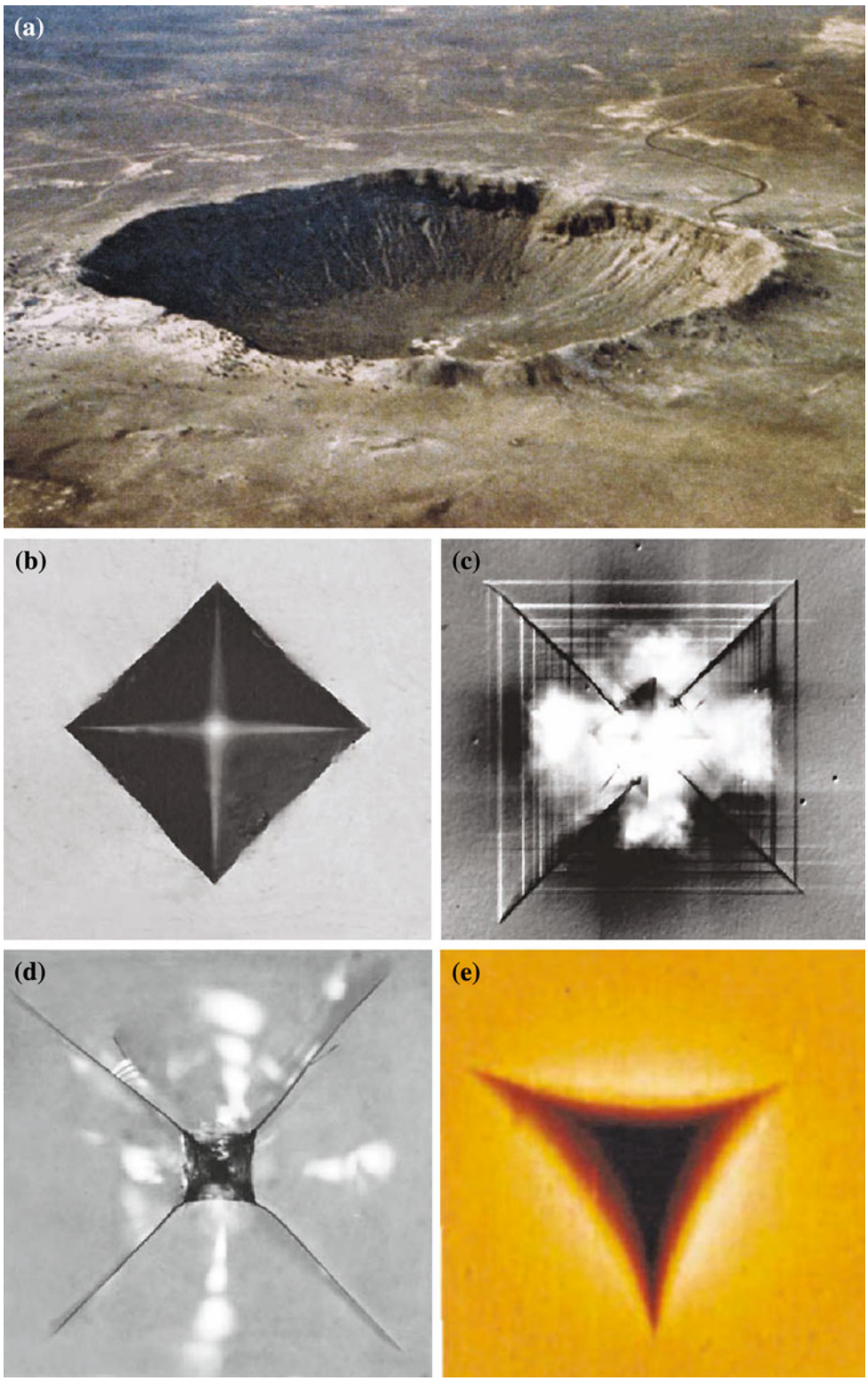

Fig. 1 Indentations in materials: **a** impact crater, Arizona; **b** Vickers indentation in steel; **c** Vickers indentation in monocrystalline (001) MgO; **d** Vickers indentation in soda-lime glass; **e** Berkovich indentation in polymethyl methacrylate. Impression sizes range from kilometre to nanometre

properties, but our emphasis will lean toward brittle solids. The versatility of the indentation methodology springs from the availability of hardness testing machines and other routine mechanical testing equipment in materials laboratories. Specimen preparation demands are minimal, requiring only a small specimen with well-polished surface to enable multiple tests. Indentation testing is one of the most versatile tools in the armoury of the materials scientist.

A key issue that arises in indentation testing is that of size. The scales for the examples shown in Fig. 1 range from kilometre to nanometre. As one progresses from contacts on the macro-scale through to the nano-scale there can be apparent changes in mechanical properties, with attendant transitions in the balance between competing damage processes [11]. Such progression is readily studied in the laboratory by progressively diminishing the contact load, in extreme cases from kilonewton to nanonewton. Systematic variations in mechanical properties, chiefly hardness, have been variously discussed in terms of an 'indentation size effect'. While widely studied, the underlying mechanisms of such effects remain a subject of debate. The ever-growing quest for an understanding of deformation and fracture mechanisms at the near-atomic level, along with the need for a properties probe for investigating small-scale specimens and devices, has led to the rise of a comparatively new branch of contact mechanics—'nanomechanics'—with the advent of dedicated nanoindenters and atomic force microscopes. The evolution of indentation techniques through the scaling spectrum is a focal element in modern-day materials science.

The layout of this article is as follows. First, we discuss testing in the region of microindentation, here loosely taken to mean contacts at loads in the vicinity of 1 N or above. In that part we make distinction between deformation and fracture, indicating how indentations may be used to evaluate basic material properties—modulus, hardness and toughness. Second, we discuss nanoindentation, for contacts around 1 N or below. Following that, the use of indentations as 'controlled flaws' in the evaluation of strength of materials is outlined. Then we consider some material aspects of indentation as they relate to structural descriptors—deformation mechanisms, microstructural interactions, rate effects, etc. Select applications in structural, functional and biological systems are cited to highlight the broad utility of indentation testing. Finally, some general conclusions are drawn, with an advocacy of the methodology as an all-inclusive exploratory tool.

Microindentation

Deformation

Consider the configuration in Fig. 2 of a flat surface loaded statically with a sharp fixed-profile indenter at an axial load P. The indenter has a fixed apical half-angle ψ (here measured from the load axis to the most remote vertex). In an ideal elastic–plastic solid the indenter creates a residual impression of characteristic dimension a (here measured from the centre to the most remote corner or edge of the impression). Hardness H may be defined in terms of contact force/projected area of indent [2]

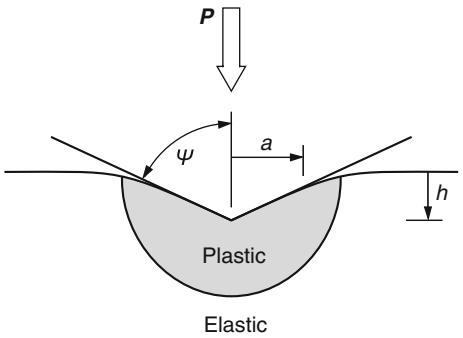

Fig. 2 Schematic diagram of elastic–plastic impression of half-diagonal a from sharp indenter of semi-apical angle ψ at axial load P and depth h

$$P/a^2 = \alpha H \tag{1}$$

where α is a shape factor: cone indenter, $\alpha = \pi$; symmetrical 4-sided (Vickers) indenter, $\alpha = 2$; 4-sided but elongate (Knoop) indenter, $\alpha = 2/7$; 3-sided (Berkovich) indenter, $\alpha = 3^{3/2}/4$. The use of *projected* rather than *actual* contact area is fundamentally more sound, because it more directly determines the intensity of stress beneath the contact [2]. Notwithstanding this, some hardness values are traditionally measured in terms of *actual* contact area, e.g. $\alpha = 2.157$ for Vickers hardness number (VHN), so some qualification of definitions is sometimes necessary.

In the rare case that the contact under the indenter is purely elastic, e.g. some rubbers, the contact relation is expressible in terms of Young's modulus E using Sneddon's relation [12]

$$P/a^2 = \left[\alpha/2\left(1-\nu^2\right)\right]E \cot \psi \tag{2}$$

with $\alpha = \pi$ for a conical indenter and ν Poisson's ratio. This equation also holds during the unloading half-cycle of most other materials, and thereby provides a basis for evaluating E ("Instrumented testing" section).

Normally for irreversibly deformable materials the indentation hardness is intrinsically related to the yield stress Y. Analysis of the contact mechanics requires simplifying assumptions concerning the nature of the deformation zone. For rigid plastic solids with negligible elastic deformation prior to yield (soft metals), material flows unimpeded around the sides of the indenter and piles up around the contact site. This kind of deformation process is well-defined by slip-line plasticity theory [10]. According to Tabor [2], the relationship between hardness and yield stress for an isotropic solid then assumes a simple, limiting form

$$H = CY \tag{3}$$

with constraint factor $C \approx 3$. For elastic–plastic materials with higher yield points (hard metals, soft ceramics) the

deformation pattern begins to resemble more an 'expanding cavity' in which the material displaced immediately beneath the indenter pushes radially outward into an elastic 'hinterland', analogous to the expansion of a hemispherical hole under internal hydrostatic pressure [13]. Materials in this class do not show plastic pile-up around the impression. The relationship between hardness and yield stress can now be expressed by Johnson's relation [14]

$$H = (2Y/3)[1 + \ln(E \cot \psi/3Y)] \quad (4)$$

Figure 3 is a plot of H/E versus Y/E, with Eqs. 2, 3 and 4 providing bounds for finite element analysis solutions. Materials with small H/E (soft metals) lie toward the lower left of this diagram, and are characterised by a plastic zone extending well beyond the contact boundary; conversely material with large H/E (hard ceramics) lie toward the upper right, with plastic zone constricted to the contact boundary.

Notwithstanding our caveats in the above contact mechanics, it may be concluded that the competition between deformation modes can be usefully quantified by the ratio of hardness to modulus H/E. This assertion is demonstrated in the degree of elastic recovery observed during a full load P versus displacement h cycle for any given material [15–19]. The lower the value of H/E the greater the component of plasticity relative to elasticity, and vice versa [16]. Recovery is effected by pushback of the elastic hinterland on the plastic zone during unloading, to a degree dependent on the partitioning of plastic and elastic deformation during preceding loading. Figure 4 depicts typical load–unload P–h curves for idealised material classes [20]: (a) an elastic solid with full recovery (rubber), (b) an elastic–plastic solid with partial recovery (hard ceramic), (c) a rigid plastic solid with zero recovery (soft metal) and (d) a viscoelastic solid with hysteretic recovery (cross-linked polymer). The presence of any unrecovered impression depth implies the existence of some residual stored stresses in the elastic region, especially in those materials that do not exhibit pile-up. The utility of depth h in place of impression size a as a characteristic contact dimension lies in its ready amenity to instrumented measurement [7, 21], foreshadowing modern-day automated nanoindentation ("Instrumented testing" section).

It is implicit in most treatments of contact mechanics that irreversible deformation is essentially a shear process, definable by a yield stress, via dislocation motion or twinning on well-defined crystallographic planes within the structure. This is not always the case. Some materials, especially those with larger values of H/E, may undergo densification by compaction or phase transformation from the intense hydrostatic compressive stresses within the immediate contact zone. Classic examples include those open-structured silicate ('anomalous') glasses without network modifiers to facilitate structural slip [22, 23], some semiconductors [24], porous ceramics [25] and foams [26] in which compaction occurs by some form of interpore microcrack coalescence or pore collapse ('cataclastic flow') [27]. Other examples include materials that undergo phase transformation under combined hydrostatic + shear

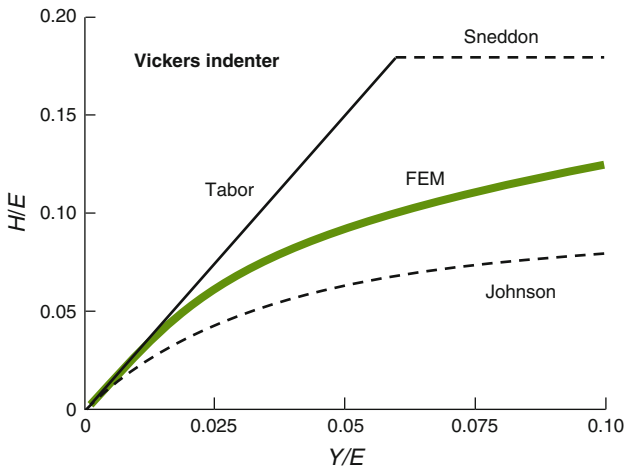

Fig. 3 Plot of hardness versus yield stress, normalised to Young's modulus, for Vickers indenter

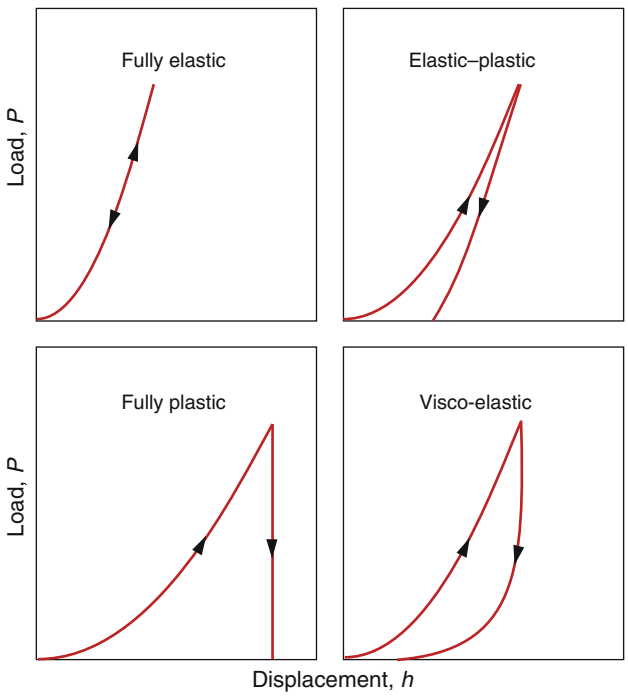

Fig. 4 Load P versus indenter displacement h for various idealised material types. Energy dissipated during cycle given by area under $P(h)$ curve

stress ("Pop-in and pop-out mechanisms" section). In such instances the volume of the indentation is more readily accommodated within the compaction zone, diminishing the intensity of any residual stresses. Polymeric materials deform with a large component of viscous flow [28]. Expanding cavity models are then no longer valid, and alternative descriptions based on a 'surface blister' concept have been used to model indentation-compaction stress fields [29]. Other complicating factors are contact friction [4], work hardening [4, 10], creep [30] and crystalline anisotropy [31].

Thus, while indentations are easy to perform, theoretical analysis is not straightforward. Much reliance has been placed on simplistic contact models which, while capturing the essence and providing explicit solutions, are subject to many assumptions and approximations. The latest trend is to solve all specific material cases by brute force numerical methods. The advantage of such a course is that modern-day computers can handle all manner of complexities in material response and contact geometries in an objective manner. However, numerical modelling is limited to case studies, providing, at best, only semi-empirical functional relations. Numerical approaches are also limited by the validity of input constitutive relations for any given material type, especially when competing deformation processes (e.g. plasticity versus densification) are involved.

Fracture

All contact fields contain some component of tensile stress, however small. This exposes the more brittle solids to cracking around the contact site—so-called 'indentation fracture' [5]. In some ceramics, the value of H/E can be as much as 0.1, corresponding to contact pressures near the theoretical limit of cohesive strength, an ideal condition for crack initiation and propagation. Prior to a burgeoning interest in ceramics in the sixties and seventies cracking around indentations was regarded as a nuisance, at most a curiosity. Indeed, the development of the Knoop indenter, with its elongate contact, was first hailed as a means for suppressing such fracture. In fact, fracture was not so much suppressed as obscured beneath the Knoop hardness impression [32]. Since then, indentation fracture has arguably become the most widely used tool in the mechanical evaluation of brittle solids.

The most common contact configuration for production of well-defined indentation fracture patterns is that of the conventional obtuse-angled ($\psi = 74°$) Vickers diamond pyramid (Fig. 1d). Different modes of cracking formed by such indenters are indicated in Fig. 5. Principal among these are radial–median cracks: radial (R) cracks grow at the surface and extend outward, usually from the impression corners; median (M) cracks form at the base of the deformation zone and extend downward into the interior [33, 34]. These cracks have a common characteristic feature: once initiated, they grow stably on an ever-expanding curved front as load increases—they tend toward a 'penny-like' geometry [35–38]. Fully developed R and M cracks are really part of the same half-penny crack system, although in some materials one mode may dominate the other. The evolution of the R–M crack system is not straightforward, as evidenced by the Vickers indentation sequence for soda-lime glass in Fig. 6. This sequence, photographed in polarised light from below, shows radial cracks forming during loading (a, b), but continuing to expand during unloading (c, d) [39]. The persistence of a bright 'Maltese cross' on completion of the cycle confirms the presence of a strong residual field from the radially expanded plastic zone, with near-centrosymmetric tensile hoop stresses—it is only the release of superposed elastic compressive (Boussinesq) stresses localised near the specimen surface that allows R cracks to expand into their ultimate half-penny shape during unloading [40]. The corresponding elastic stresses in the subsurface region are actually tensile, so M cracks usually attain their maximum depth at full load. The degree to which R lags M crack development during the cycle depends on the relative strengths of the elastic and plastic components of the contact field [7, 40]: for materials with large H/E the degree is more pronounced, while for materials with small H/E it is less so.

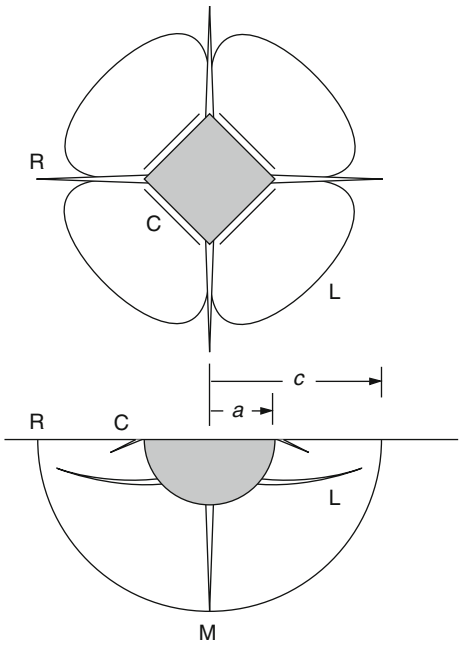

Fig. 5 Crack patterns around plastic zone in brittle solid: *M* median crack, *R* radial crack, *L* lateral crack, *C* peripheral crack

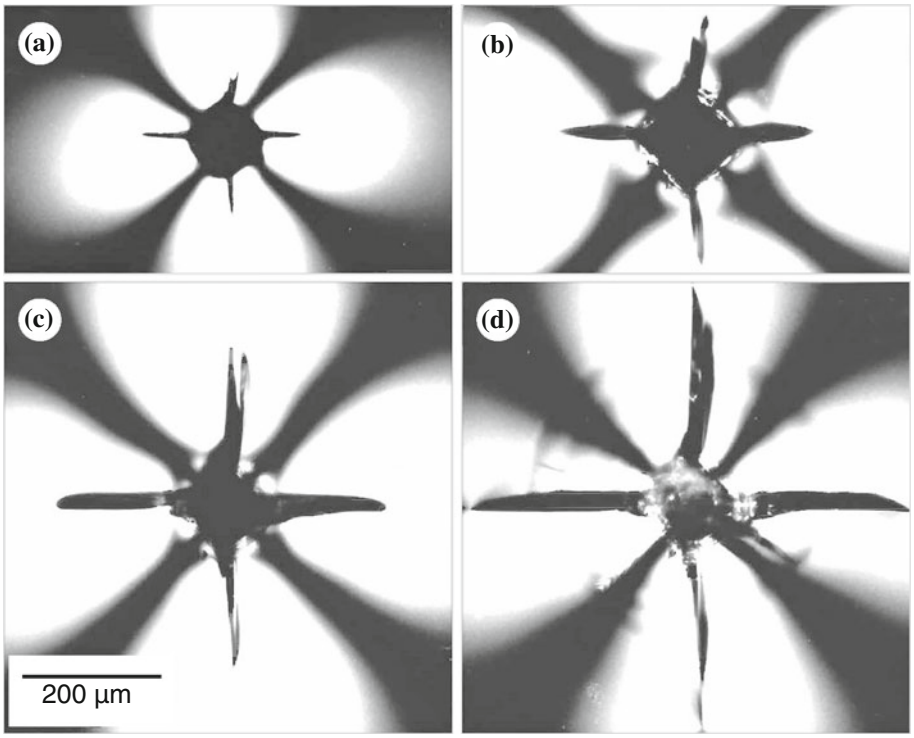

Fig. 6 Sequence showing evolution of radial crack in soda-lime glass during contact with Vickers indenter: **a** partial load, **b** full load, **c** partial unload, **d** full unload. Photographs taken in situ from below indenter in polarised light. Note extension of cracks in **c** and persistent birefringence in **d**, indicating existence of residual tensile stress component in the contact field. Subsurface lateral crack is faintly visible as near-circular fringe pattern in **d**. From [39]

Another fracture mode is the lateral crack (L) [7, 33, 41]. Lateral cracks initiate from the sides of the deformation zone and expand outward and upward into a shallow saucer configuration, again largely during unloading. They are faintly visible as the near-circular fringe pattern in Fig. 6d. In opaque materials they are identifiable by surface uplift immediately surrounding the indentation or (in extreme cases) where they intersect the surface by remnant surface scallops. Lateral cracks have been modelled as a flexing disk anchored at the base of the plastic zone, with somewhat more complex fracture mechanics [41]. They are useful in the modelling of wear and erosion of brittle surfaces from multiparticle contacts [42]. Peripheral cracks near the edge of the impression (C) are also evident in some materials, somewhat analogous to cone cracks observed around blunt indenters [9] but generally much shallower.

Notwithstanding its complex evolution, the fully developed R–M crack is amenable to rigorous fracture mechanics analysis. In the absence of rate effects (see "Indentations as controlled flaws" section), the unloaded crack is in a state of stable equilibrium within the residual stress field. Its geometry is effectively that of a centre-loaded half-penny [35], resulting in a characteristic relation between load P and corner crack length c (Fig. 5)

$$P\Big/c^{3/2} = (1/\xi)(H/E)^{1/2}T \tag{5}$$

where T is toughness (K_{IC} in engineering parlance) and $\xi = \xi_0(\cot\psi)^{2/3}$ is an angle-dependent dimensionless quantity, with ξ_0 an angle-independent quantity [40]. Note again the appearance of the ratio H/E. A critical analysis of Vickers indentation data for a range of glasses and ceramics provides a coefficient $\xi = 0.016$ [43]. It is implicit in En. 5 that the material is ideally elastic–plastic with a radially expanding deformation zone and that it is homogeneous and isotropic. Such conditions are not always met, e.g. anomalous glasses, large-grain ceramics, anisotropic monocrystals [43]. There have been several variants on this approach, some simply presenting 'improved' evaluations of ξ, others suggesting slightly modified forms of Eq. 5. Still others, based on different crack geometries, e.g. shallow semi-elliptical 'Palmqvist' cracks [44], offer alternative relations between P and c and differing dependencies on H/E [45, 46]. Such variants have been usefully tabulated by Ponton and Rawlings [47, 48].

One of the most widespread uses of indentation fracture in brittle solids is the measurement of toughness. Relations of the kind in Eq. 5 provide a quick and economical route—simply measure the surface lengths of R cracks at the corners of Vickers indentations and deconvolute T [40, 44, 49]. All that is required is a well-behaved R crack pattern on a smooth surface, ideally with $c > 2a$ (Fig. 5). It is its simplicity that has seen indentation fracture become the most widely used of toughness tests in brittle materials, notwithstanding its perceived vulnerabilities (diversity of equations, departures from ideal crack geometries, sensitivity to nature of plastic zone). The user needs to be cognizant of both advantages and disadvantages of the technique [43, 47, 48].

One quantity that has proved elusive is that of 'brittleness'—how may one quantify the competition between fracture and deformation in the mechanical response of a solid? A simple measure follows from the different load dependencies of plastic impression dimension a and radial crack dimension c in Eqs. 1 and 5 [50, 51]. Physically, this difference in dependencies is attributable to the fact that fracture occurs on a surface (dimension^2) while deformation occurs within a volume (dimension^3). Illustrative data for soda-lime glass and single crystal sapphire are plotted in Fig. 7. The fitted $P(a)$ and $P(c)$ lines intersect at $a^* = c^*$, obtained by inserting $P = P^*$ into Eqs. 1 and 5:

$$a^* = (1/\alpha\xi)^2 T^2/EH \tag{6}$$

And so we have an intrinsic size effect: above the threshold, fracture dominates; below it, deformation dominates. Metals and polymers have relatively large values of a^* and P^*, ceramics have small values. The existence of a threshold explains why brittle solids undergo wear by microfracture in contacts with coarse particles (grinding) and by microdeformation with fine particles (polishing). From a micromechanics perspective, the fracture threshold can be described in terms of initiation from deformation-induced or pre-existing crack nuclei. In homogeneous, isotropic materials—normal glasses and fine-grain polycrystals—these nuclei take the form of 'shear faults', discrete slip events defined by trajectories of maximum shear stress within the deformation field [36, 52–55]. Shear fault traces at a section through a Vickers indentation in a glass are shown in Fig. 8. Cracks can initiate either from extensions of these faults into the underlying tensile field or, more likely, from stress concentration sites at fault intersections, depicted in Fig. 8b. In single crystals, the slip planes and ensuing cracks tend to be constrained to favoured crystallographic planes. Insofar as the intensity of the indentation stress field is load invariant (H independent of P), the critical condition for initiation is that the shear fault should grow to some critical size ($a \propto P^{1/2}$) [56]. In coarse-grain structures the microstructure itself can provide initiation sources (e.g. pores, weak grain boundaries). More detailed micromechanical models of crack initiation within the indentation field confirm the existence and essential form of the threshold condition in Eq. 6 [51, 53, 54, 56].

There is room for more objective analysis of indentation fracture, e.g. using the latest extended finite element models. Such packages have the potential to accommodate all manner of geometrical and material complexities—crack configuration (radial–median, lateral), indenter type (shape, angle), deformation mode (plasticity, compaction) and material anisotropy (crystallographic, microstructural). However, such methods should be seen as a complement, not a replacement, for analytical models.

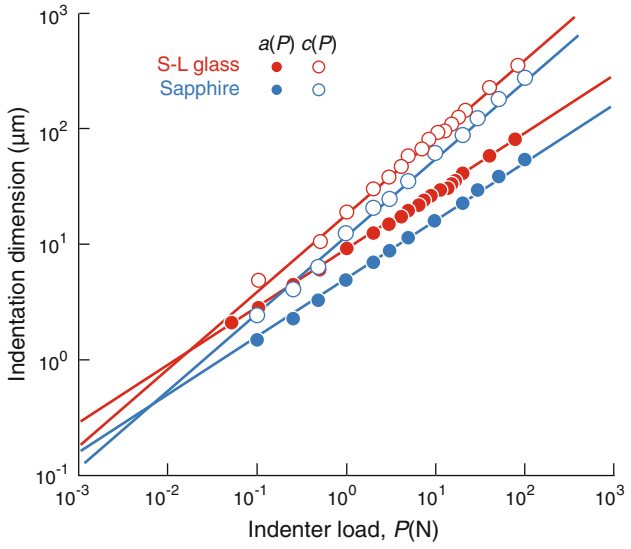

Fig. 7 Vickers indentation dimensions a and c as function of load P, data for soda-lime glass and sapphire single crystal. Intersection of curves indicates brittle–plastic transition. Data from [50, 183]

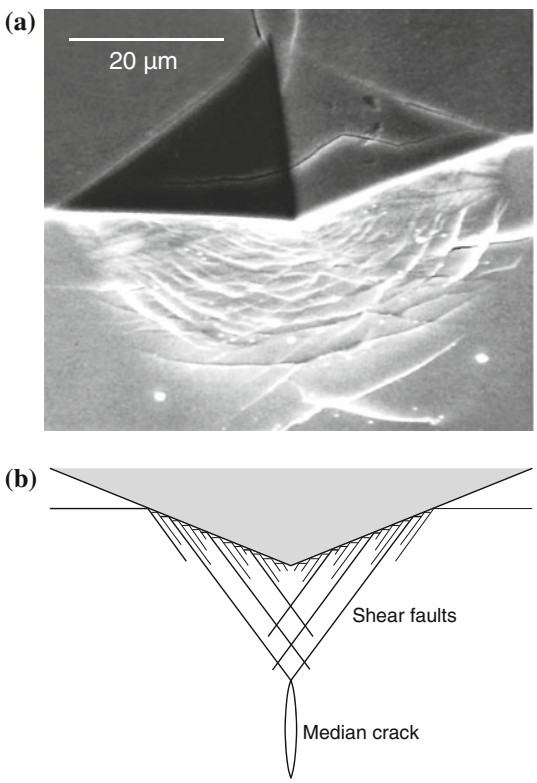

Fig. 8 **a** Section through Vickers indentation in an arsenic trisulphide glass at load $P = 2$ N. Deformation is accommodated by 'shear faults' beneath the contact. Courtesy T.P. Dabbs. **b** Schematic diagram indicating how shear-fault or slip-line intersections generate median cracks beneath the contact axis (or radial cracks at the surface)

Nanoindentation

Instrumented testing

The last two or three decades have witnessed an explosion of interest in 'nanoindentation', driven by a continuing push toward small-scale material and thin film systems [57]. This explosion has become so focussed that nanoindentation operators have formed a community of their own. Nanoindentation is distinguished from its more traditional predecessors by a shift in measurement paradigm, from direct measurement of contact area to depth sensing. This shift has evolved partly to avoid the increased impracticality of contact area measurement at low loads but, more importantly, because of the amenability of depth measurement by precision transducers [58]. The latter lends itself to electronic automation. There are now several commercial instrumented nanoindentation testing machines available on the market. Inbuilt software enables recording and analysis of complete load–unload $P(h)$ data through one or more contact cycles (Fig. 4). Most instruments have the capacity to place extended arrays of contacts at preselected locations on a specimen surface, with some form of microscope facility (including AFM) to view the indentations after the event. Additional facilities include sliding contacts (scratch testing), frequency-imposed oscillatory force modulation (energy dissipation in polymers), stiffness mapping, acoustic emission and replacement of sharp indenters with small spheres (adhesion measurement) [59].

Another distinguishing feature of nanoindentation is a shift from 4-sided to 3-sided indenters, primarily because of a greater ease in fabricating indenters with sharp tips. The most common nanoindenter geometry is the Berkovich ($\psi = 77°$), with half-angle similar to Vickers ($\psi = 74°$). (The Berkovich and Vickers geometries have the same 'equivalent cone' angle 70.3°.) Also widely used is the more acute cube-corner indenter ($\psi = 42.3°$), introduced by Pharr in order to facilitate evaluation of indentation toughness in smaller specimens [60, 61]. Pharr found that Eq. 5 remains valid for cube-corner indenters but with a substantially larger coefficient $\xi = 0.040$, thereby resulting in much diminished values of a^* (and P^*) in Eq. 6 [60]. In a more detailed study, Morris and co-workers investigated the role of indenter angle over a range of ψ [62–64] and reported some distinctive changes in deformation and fracture patterns. An example is shown in Fig. 9 for indentations at a common load 200 mN in soda-lime glass. For the more acute indenters, those authors noted an increase in pile-up around the indentations and a greater incidence of radial cracking. They argued that the expanding cavity model implicit in Eq. 5 no longer applies to acute indenters and that the driving force for fracture in those cases may come more from a crack-wedging component in the loading [62–64]. Nonetheless, the basic penny crack $P/c^{3/2}$ dependency in Eq. 5 continues to holds in all these configurations.

Building on the descriptions of elastic recovery described earlier, many attempts have evolved in an attempt to analyse the $P(h)$ function, with an express aim of

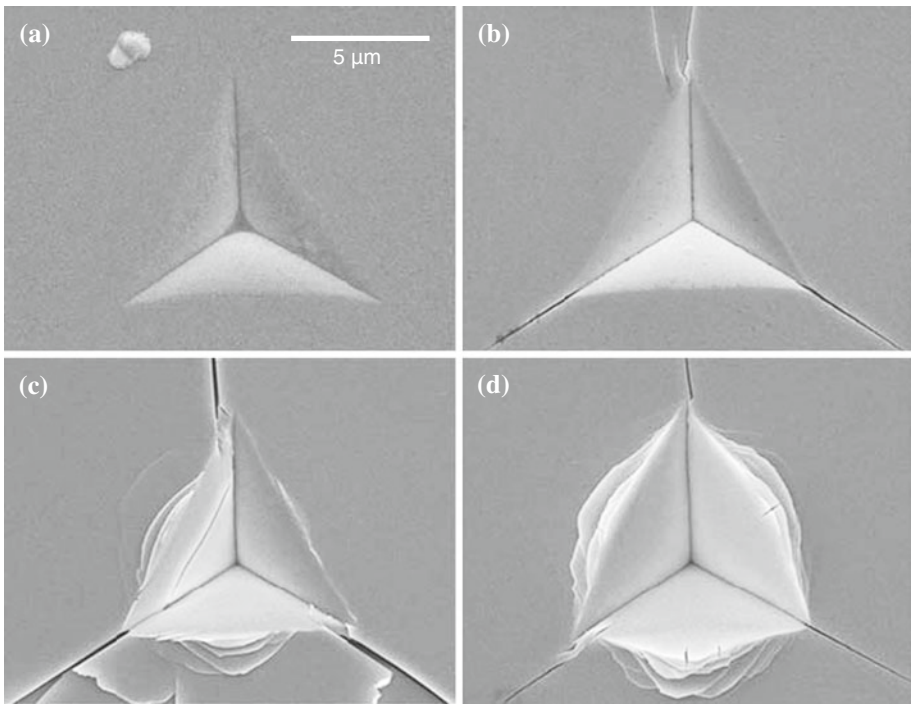

Fig. 9 Residual impressions in soda-lime glass from 3-sided diamond indenters of different acuity, at load 200 mN: **a** Berkovich ($\psi = 77.0°$), **b** custom indenter ($\psi = 68.8°$), **c** custom indenter ($\psi = 61.3°$), **d** cube corner ($\psi = 54.7°$). Scanning electron microscope images. Note increasing incidence of pile-up and corner cracking with decreasing ψ. From [64]

deconvoluting characteristic material properties. The most widely adapted of these is that by Oliver and Pharr [58], derived from Sneddon's relation in Eq. 2. Hardness H and 'reduced' modulus E_r are measurable from the elastic–plastic loading and unloading half-cycles, respectively:

$$H = P_m/A \tag{7a}$$

$$E_r = (\pi/A)^{1/2} S/2 \tag{7b}$$

with projected contact area $A = A(h)$ a semi-empirical function and $S = dP/dh$ a 'stiffness' measured at the onset of unloading [58, 65]. The reduced modulus is related to the Young's modulus E by $1/E_r = (1 - \nu_i^2)/E_i + (1 - \nu^2)/E$, with subscript i denoting indenter. The quantities H and E_r in Eq. 7 are usually extracted by the machine software.

The advantages of automated indentation testing are eminently apparent and account for the widespread use of the methodology today. On the surface, its computerised operation would appear to make measurement simple and objective. However, there is an element of 'black box' in the technology that can lead the untrained practitioner astray. It is crucial that due attention be paid to potential artefacts—instrument calibration, thermal drift, pile-up or sink-in, surface roughness, tip rounding, tip adhesion and so on [57]. Nanoindentation is a lot more than simply pushing a button.

Small-scale deformation and size effects

As indicated earlier, traditional contact deformation theory for fixed-profile indenters has been largely developed on the presumption of geometrical similarity, i.e. hardness H independent of load P [2]. Along with the advent of nanoindentation has come mounting evidence that this condition can break down. Most often in such instances H tends to increase as indentation size diminishes into the nano domain, to a degree dependent on the class of material. Initial attempts to explain this behaviour were directed toward extrinsic causes [66]: oxide or other surface layers, machining and polishing damage, residual stresses and contact friction. However, size effects are apparent in even the best-behaved and best-prepared materials, indicating some intrinsic contribution.

Perhaps the most widely quoted model accounting for an intrinsic dependence of hardness H on indent size is that of Nix and Gao [67]. Those authors describe a competition between 'randomly stored' and 'geometrically necessary' dislocations. The argument goes that the density of geometrically necessary dislocations, those needed to accommodate the volume of the indentation, increases as depth h diminishes, leading to the following $H(h)$ dependence:

$$H = H_0(1 + h^*/h)^{1/2} \tag{8}$$

where H_0 is an asymptotic high-load (P-invariant) hardness and h^* is a transition depth dependent on shear modulus, average shear strain within the deformation zone and indenter angle. An example, showing a fit to data for silver single crystals [68], is plotted in Fig. 10. The value of h^* is typically much larger for metals than for ceramics. The model is somewhat phenomenological, with a basis in continuum 'strain gradient' theory [69].

Considerable work has been conducted over the years on the observation of actual dislocation activity beneath sharp indenters in the electron microscope, on an ever-decreasing scale [32, 70–77]. At low-load indentations in brittle materials like silicon, dislocations appear as well-spaced, discrete loops, as seen in the transmission electron images in Fig. 11. Some stress relief must accompany the pop-in of any single loop, necessitating a further increase in contact area to rebuild the stress in order to nucleate the next loop. This element of discreteness in the plasticity process may go part way to explain an increased hardness in the nanoindentation domain, as the probability of locating dislocation sources within an ever-smaller volume diminishes with decreasing load.

Pop-in and pop-out mechanisms

Apart from offering simple measurements of modulus and hardness, nanoindentation is uniquely placed to provide fundamental information on the way materials undergo structural phase transformations under intense compression. Such transformations are of special interest in small-scale semiconductor devices, where damage at stress-concentrating contacts can lead to system failure. Phase

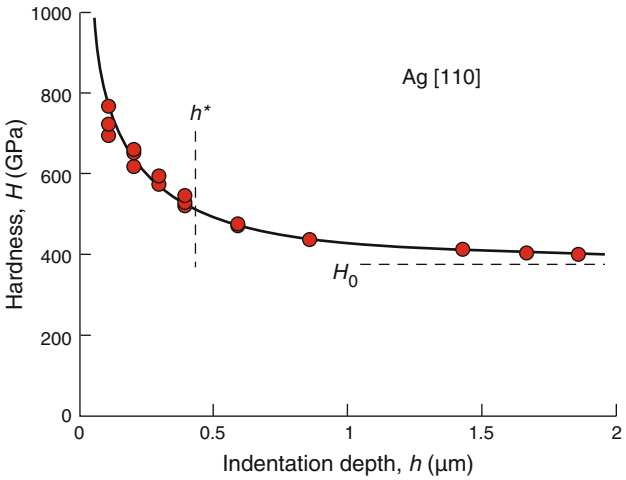

Fig. 10 Hardness as a function of nanoindentation depth for Ag single crystals, showing indentation size effect. Plot from [67] using data from [68]

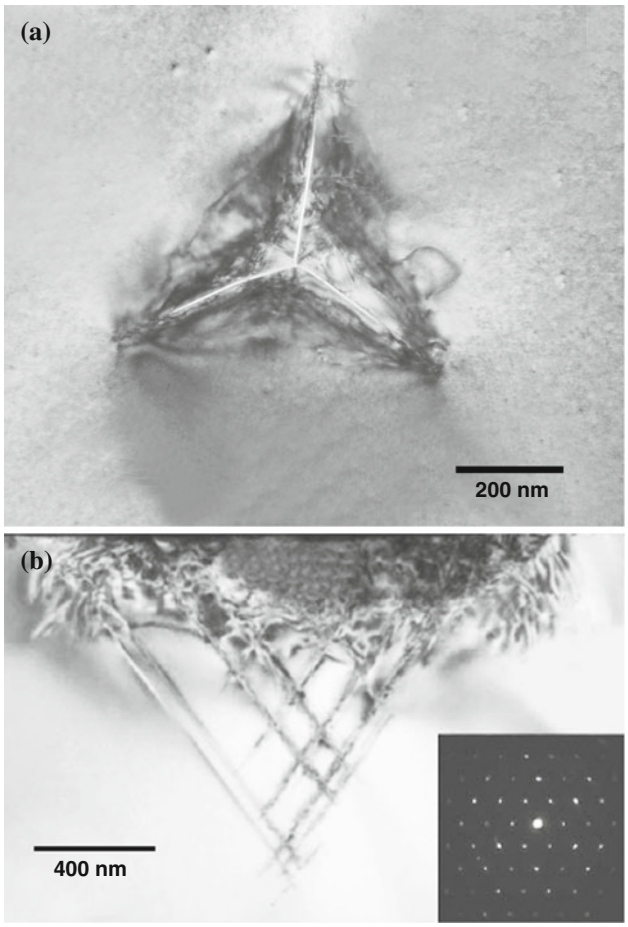

Fig. 11 Transmission electron micrographs of nanoindentation sites in Si single crystals. **a** Surface view, indentation load $P = 5$ mN. Specimen prepared by ion beam machining of indented surfaces from below. Note dislocation loops around immediate contact site. Image courtesy B.J. Hockey. **b** Side view, indentation load $P = 30$ mN. Thin section machined by focussed ion beam milling. From [77]. Intersections of slip faults are favoured sites for crack initiation (cf. Fig. 8b)

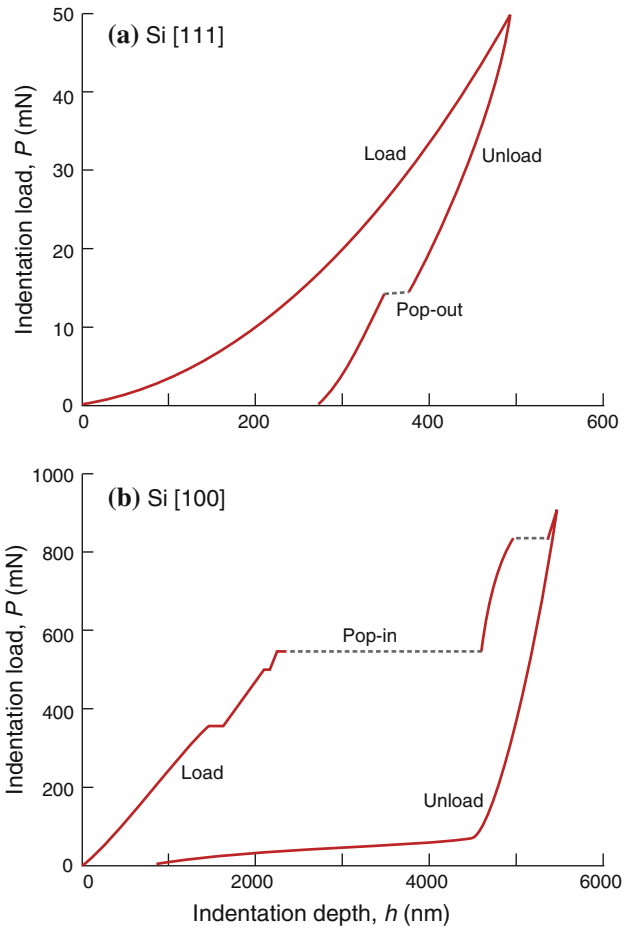

Fig. 12 Load–displacement curves for single crystal Si with Berkovich indenter, up to different maximum loads: **a** $P_m = 50$ mN [79], showing pop-out due to phase transformation; **b** $P_m = 1000$ mN, showing pop-in due to lateral crack spallation [184]

transformations in semiconductor materials were first reported by Drickamer and colleagues using an engineering-scale high-pressure apparatus [24], and subsequently by Piermarini and Block [78] using compact diamond anvil cells. But those types of equipment are available only in highly specialised laboratories and are costly to operate. Nanoindentation also generates sufficiently high levels of hydrostatic compression to activate transformations but with much wider accessibility and more economical operation. It is in this context that the use of nanoindentation to identify and quantify phase transformations in semiconductors and other materials has expanded dramatically over the last two decades [72, 73, 75, 76, 79–81].

The clearest manifestation of a phase transformation in a nanoindentation experiment is the appearance of a distinctive displacement excursion or load drop in the $P(h)$ curve, depending on the system compliance. Some events are less distinctive, marked by an 'elbow' in the curve. These events can occur on loading (pop-in) or unloading (pop-out). An example of pop-out in single crystal silicon indented at low load is shown in Fig. 12a. This particular excursion is attributable to stochastical nucleation of a pressurised Si-II phase (transformed from Si-I almost immediately on loading) to less dense Si-III and Si-XII phases [79]. Silicon exhibits such transformations more than any other material studied to date, and for this reason (in addition to its importance in the semiconductor industry) has drawn the lion's share of attention in the nanoindentation community. An armoury of analytical techniques—transmission electron diffraction, Raman spectroscopy, electrical resistance, etc.—has helped identify several crystalline and amorphous phases [80, 82].

Additional, pop-in displacement excursions can be caused by the initiation of individual slip bands, cracks or other irreversible processes. An extreme example is given

in Fig. 12b, showing a 'giant' pop-in attributable to the sudden spallation of a lateral crack [83]. These events have not received the same degree of attention as phase transformations.

Controlled indentation flaws and strength degradation

Indentations as controlled flaws

The strength of real materials is governed by the ubiquitous presence of microscopic or submicroscopic defects or flaws: in metals, predominantly dislocation slip bands or faults [84]; in ceramics, microcrack-like stress raisers [85]. A single defect in an otherwise 'perfect' solid can diminish strength by orders of magnitude relative to the upper theoretical limit calculated from bond force laws [86]. These defects are typically distributed in broad populations, often necessitating some form of stochastic treatment. It is in this context that indentations can provide insight into the intrinsic strength properties of materials, by serving as 'controlled flaws' [87]. An indentation can be placed in the surface of a specimen to create a critical flaw at a predetermined location, thus enabling direct observation of the micromechanics of flaw evolution during subsequent tensile loading [39]. The sensitivity of strength to flaw size can then be investigated by systematically varying the indentation load [88]. Moreover, material properties can be deconvoluted from strength data, with less reliance on statistical analysis.

Here we focus on brittle solids containing indentation flaws in the postthreshold region of Fig. 7, leaving consideration of subthreshold flaws to the next subsection. The origins of flaws in this class of material are diverse, ranging from spurious surface handling defects in glasses and single crystals to internal sources of microstructural weakness or stress concentration in polycrystalline ceramics [89]. The Griffith theory of strength [85] states that brittle fracture initiates spontaneously from a flaw of characteristic dimension c at a critical tensile stress $S = T/\lambda c^{1/2}$, with λ a crack geometry constant. This presumes the absence of any rate-dependent crack growth from interaction with a chemically active environment, especially water (see "Rate effects" section), in which case the quantity S defines an 'inert strength'. Consider an indentation flaw with radial–median (R–M) crack of dimension c formed at load P (Fig. 5), and neglect for a moment the existence of any residual contact stresses from the plastic zone. In combination with Eq. 5 we may directly eliminate c to obtain a strength equation in terms of P:

$$S = (\varsigma/\lambda)T^{4/3}/P^{1/3} \tag{9a}$$

where $\varsigma = (1/\xi^{1/3})(H/E)^{1/6}$. In reality, residual contact stresses persist at indentation flaws during subsequent tensile loading, providing a superposed driving force that needs to be taken into account in the fracture mechanics [88]. Because the residual contact field declines rapidly with distance from the plastic zone, this extra driving force falls off with radial distance, causing the crack to extend stably with increasing load to about twice its immediate post-contact size before attaining instability. Such a precursor stage of stable crack growth is a distinguishing feature of cracks in localised stress fields. The ensuing strength equation retains the same form as Eq. 9a, but with a modifying factor:

$$S = (3\varsigma/4\lambda)T^{4/3}\Big/P^{1/3} \tag{9b}$$

Failure is now 'activated' rather than 'spontaneous'. Reversion to Eq. 9a can be effected by annealing out the residual stresses or polishing away the plastic zone prior to strength testing, but those are unnecessarily onerous preparation procedures.

Indentation–strength testing is appealing for a variety of reasons. It provides insight into the evolution of many natural flaw systems because of the facility for in situ observation of crack extension from initiation to failure, with far more information on the fracture process than can be gained by post-mortem fractography [89]. It usefully quantifies the sensitivity of material strength to degradation from any prospective contact event—scratches, machining flaws, particle impacts and so on [90–94]. Illustrative strength data for select brittle materials with controlled Vickers indentation flaws are plotted in Fig. 13, with solid line data fits to Eq. 9b. Horizontal dashed lines indicate strength cutoffs above which natural flaws dominate indentation flaws. The methodology also offers an alternative route to toughness evaluation, by direct deconvolution from the data fits. A major advantage is that the strength relation involves load P rather than crack size c, and is therefore much less susceptible to measurement error. Note that the coefficient ς in Eq. 9 is especially insensitive to any uncertainties in values of H/E and ξ. Moreover, the resistance to fracture for any given material may be simply assessed from the relative position on strength degradation plots like Fig. 13, without any need for toughness evaluation. In addition, the characteristic sizes of natural flaws may be determined from the loads at which the solid and dashed lines intersect in Fig. 13, again without knowledge of toughness. The main disadvantage of the procedure is the restriction to one result per specimen, a drawback common to all strength testing protocols.

There are variants on the method, e.g. the placement of multiple 'dummy' indentations in any given specimen surface to determine the critical crack size at failure, circumventing any uncertainties in crack geometry coefficient λ in Eq. 9 [95].

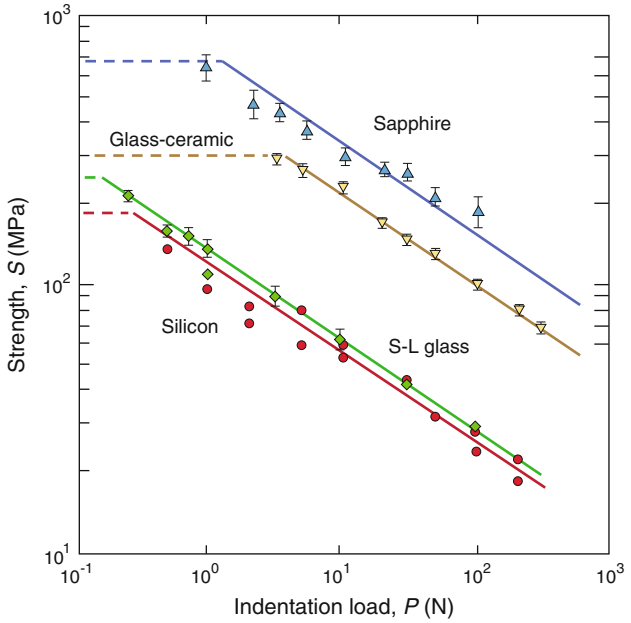

Fig. 13 Strength as function of indentation load for select materials containing Vickers indentations with radial–median cracks. All data points represent failures from postthreshold indentation sites, with standard deviation *error bars* where multiple tests have been conducted. *Solid lines* are fits to Eq. 9. Horizontal *dashed lines* are cutoff levels above which strength is dominated by natural flaws

Size effects in strength behaviour

The strength degradation analysis in the preceding subsection applies strictly to postthreshold indentations, i.e. indentations with well-formed R–M cracks. But what about indentation flaws in the subthreshold region? Images of Berkovich nanoindentations in glass, silicon and sapphire immediately on either side of the threshold are shown in Fig. 14 [96]. Note the absence of any visible corner cracks at the subthreshold impressions. Is it conceivable that such deformation-dominated indentations could cause premature failure in subsequent tensile loading? Early strength tests by Dabbs and co-workers on pristine silicate glass fibres and etched glass rods containing ostensibly crack-free Vickers indentations indicated that this is indeed the case [97, 98]. Recall from the side view images for glass in Fig. 8 and silicon in Fig. 11 that deformation zones are made up of discrete subsurface shear faults or slip bands, and that these faults act as effective nucleation sites for R–M crack initiation. Thus it seems that even the most innocuous of damage sites has the potential to degrade strength properties.

To quantify this assertion, Fig. 15 plots strength data for highly polished silicon and sapphire with Berkovich nanoindentations as a function of load, analogous to Fig. 13 but now extended into the subthreshold domain [96, 99]. The filled data points are verified spontaneous failures from subthreshold indentations, the unfilled points are activated failures from postthreshold indentations. The data points in Fig. 15, even those for subthreshold indentations, lie well below the theoretical cohesive limits for defect-free materials, confirming significant strength degradation. Assuming spontaneous initiation from an 'incipient microcrack' (discrete shear fault or slip band) of size determined by the contact dimension ($c = a$), and a

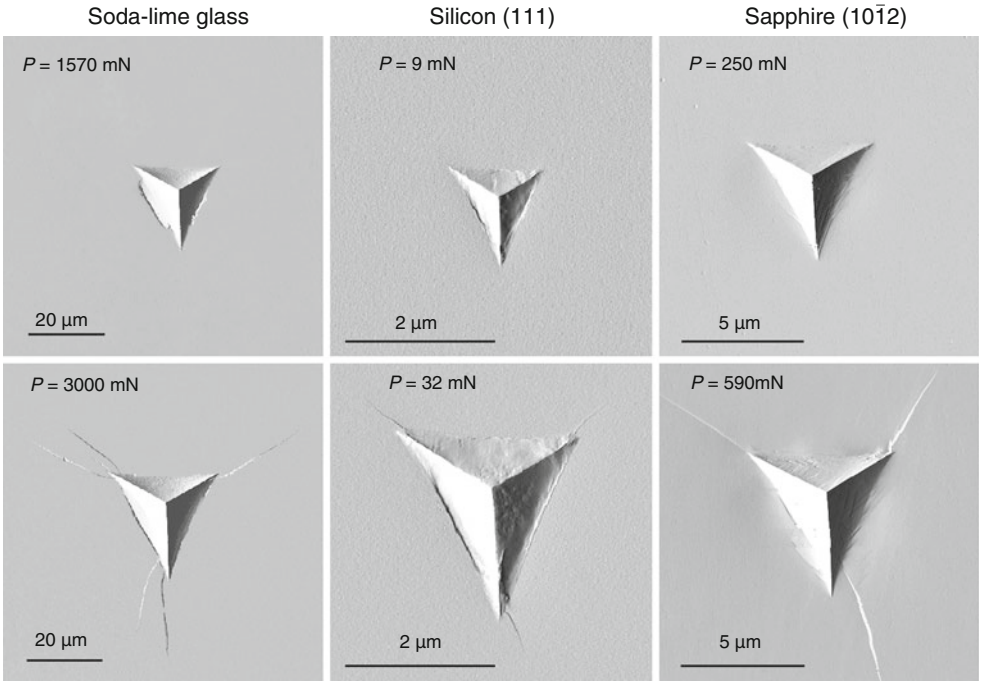

Fig. 14 AFM images of Berkovich indentations in soda-lime glass, silicon and sapphire single crystals, at subthreshold loads (*upper*) and postthreshold loads (*lower*)

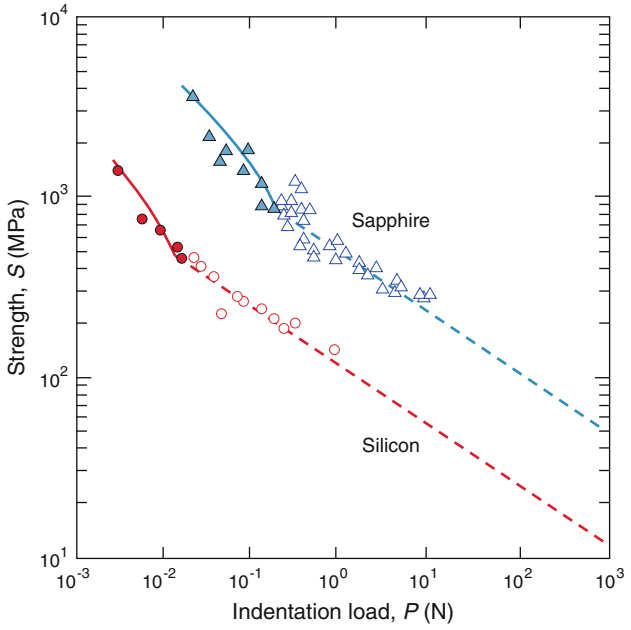

Fig. 15 Strength for select materials containing Berkovich indentations. *Filled symbols* are failures from subthreshold indentation sites, *unfilled symbols* from postthreshold sites, as function of indentation load. *Solid lines* are subthreshold fits from Eq. 11, *dashed lines* are from postthreshold fits in Fig. 13. Theoretical strength limits for each material lie above the upper bound of plot

residual field of intensity proportional to the contact pressure or hardness H (Eq. 1), fracture mechanics yields [96]

$$S = (1/\lambda)[(\alpha H/P)^{1/4}T - \kappa H] \tag{10}$$

with κ another crack geometry coefficient. Note the appearance of H in addition to T in this relation, emphasising the role of the plasticity field. The solid curves through the subthreshold data are fits to this relation; the dashed linear portions in the postthreshold region are taken from the fitted Vickers data in Fig. 13. It is notable that although the subthreshold strength levels lie above the extrapolated postthreshold line, there is no abrupt discontinuity associated with the transition.

It can be concluded that otherwise strong brittle materials are susceptible to minute nanocontacts, even in initially 'perfect' materials like dislocation-free silicon and pristine optical glass fibres, a result highly relevant to small-device applications where reliability is a paramount concern.

Other materials factors

Rate effects

Our discussions so far have implicitly assumed equilibrium conditions in the indentation deformation and fracture mechanics. This is not the norm; kinetic effects abound. They are manifest in the deformation properties as indentation creep or time-dependent hardness. Whereas in metals [30, 100] and ceramics [101] indentation creep may be considered relatively minor, the same is certainly not true of polymers. In these latter materials the mechanical response is largely viscoelastic; time dependence is of the essence. An indentation at fixed load in a soft polymer can more than double its size in a matter of minutes. Typical indentation creep data for three polymers are plotted in Fig. 16, showing (a) load–displacement $P(h)$ curves and (b) indenter displacement as a function of hold time at peak load [28]. The extent of creep depends on the degree of cross-linking in the polymer structure. Analysis of the indentation cycle for viscoelastic solids is more complex than for quasistatic elastic–plastic materials, and phenomenological rheology models are often employed to facilitate a mechanical description. By superimposing an oscillatory component in the loading, it is possible to deconvolute 'real' (storage) and 'imaginary' (loss) components of the complex elastic modulus $E = E' + iE''$ from machine stiffness data [102, 103]. With a surging interest in soft tissue engineering [104], ever more attention is being devoted to indentation micromechanics in this class of deformable materials.

Rate effects are also evident as moisture-enhanced fracture events at postthreshold indentations in ionic–covalent glasses and ceramics [105, 106]. If moisture is excluded from the test chamber, e.g. by flushing with dry nitrogen gas, the crack configuration at full unloading (e.g. Fig. 6d) remains immobile over time. But the moment laboratory air is admitted, the radial cracks accelerate outward, slowing steadily over time, ultimately more than doubling in size [43, 107]. Typical R crack data for postthreshold Vickers indentations in soda-lime glass are shown in Fig. 17a. (Lateral cracks expand more slowly, but eventually catch up.) Even trace quantities of water in nominally dry environments like silicone oil can facilitate growth, albeit at a much reduced rate. The crack growth is then governed by a velocity function, commonly written in power-law form $v = v_0(K/T)^n$, where K is a stress intensity factor and v_0 and n are constants [105, 106]. The exponent n, which quantifies the susceptibility of a given material to environmental interaction, can be readily evaluated from such data [108]. Rate effects are also manifest at subthreshold indentations, as delayed R crack pop-ins well after completion of the indentation cycle. As seen in Fig. 17b, the lower the contact load the greater the delay [55, 109]. In this case the kinetics is attributable to rate-limited intrusion of moisture into newly generated shear faults (Fig. 8a), augmenting the crack initiation process.

Sustained growth of flaws during subsequent tensile loading leads to reductions in strength over time, i.e.

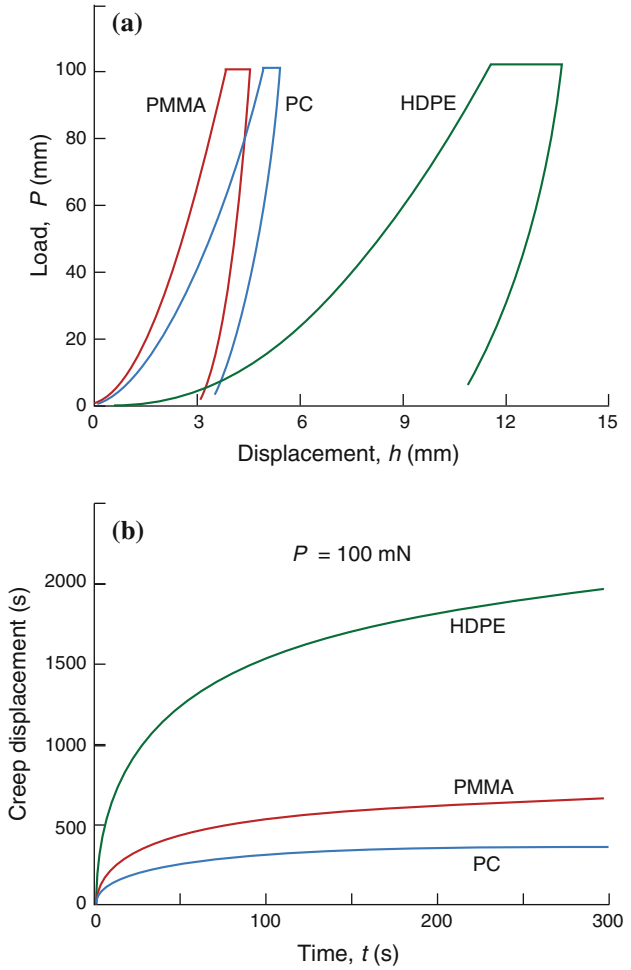

Fig. 16 Nanoindentation behaviour for three polymers, PMMA (polymethyl methacrylate), PC (polycarbonate) and HDPE (high-density polyethylene): **a** Load–displacement $P(h)$ curves; **b** indenter displacement as a function of hold time at peak load. After [28]

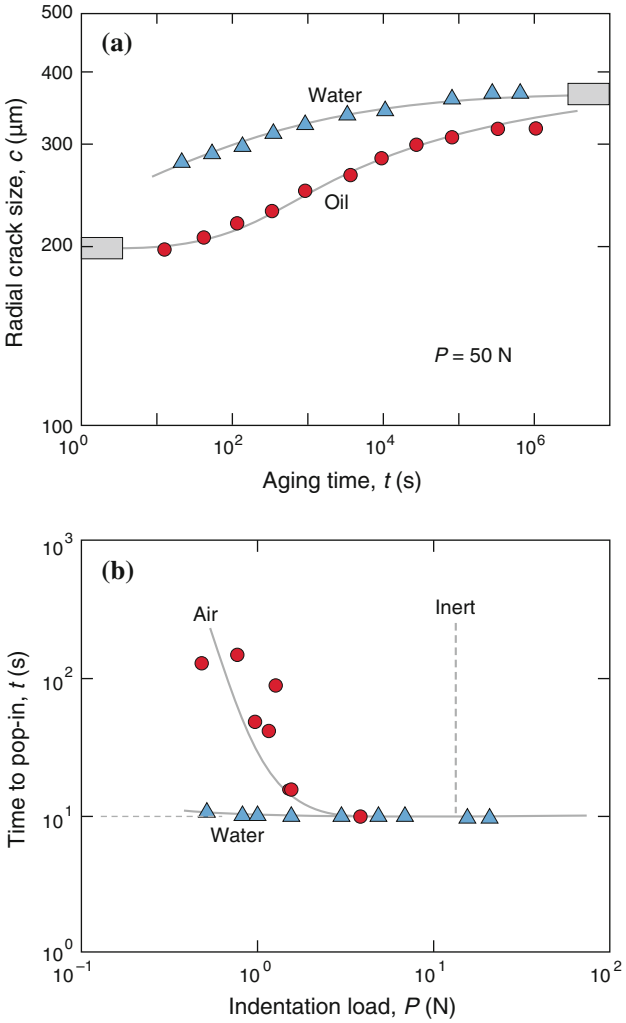

Fig. 17 Kinetic radial crack growth at Vickers indentations in soda-lime glass. **a** From postthreshold indentations at $P = 50$ N in water and silicone oil, showing crack extension with time after completion of load cycle. Shaded boxes denote initial (*left*) and final (*right*) crack sizes. Data from [185]. **b** From subthreshold indentations in water, air and inert environment (*vertical dashed line*), showing delayed pop-in time measured from the start of a 10 s contact, as function of contact load. Data from [109]

'fatigue'. The most common form of fatigue testing is that at constant stressing rates $d\sigma/dt = \sigma_t$ ('dynamic fatigue'). Dynamic fatigue relations for glasses and fine-grain ceramics containing postthreshold indentations are obtained by solving a crack velocity differential equation, with a residual stress term incorporated into the stress intensity factor [110–112]. For postthreshold indentations formed at load P the strength is given by

$$SP^{1/3} = (A'\sigma_t P)^{1/(n'+1)} \tag{11}$$

where A' and $n' = 3n/4 + 1/2$ are characteristic quantities for a given material. Load-normalised data for soda-lime glass containing postthreshold Vickers flaws in water are plotted in Fig. 17 [113]. The crack velocity exponent n can be extracted directly from fits to these data, with considerable accuracy and again without any knowledge of toughness. Included in Fig. 18 are data for subthreshold Vickers flaws [114]. Although a rigorous fatigue analysis is not available for such flaws, it is noteworthy that the data also satisfy Eq. 11, albeit with greater strength values, greater scatter and smaller n'. The value of such dynamic fatigue testing is that it provides essential crack velocity parameters for predicting chemically assisted strength degradation in any alternative engineering stress state, including those pertaining to static and cyclic loading [112]. Typically, for most glasses and fine-grain ceramics under some form of sustained loading, strengths degrade by a factor of 2 or 3 over a year [115].

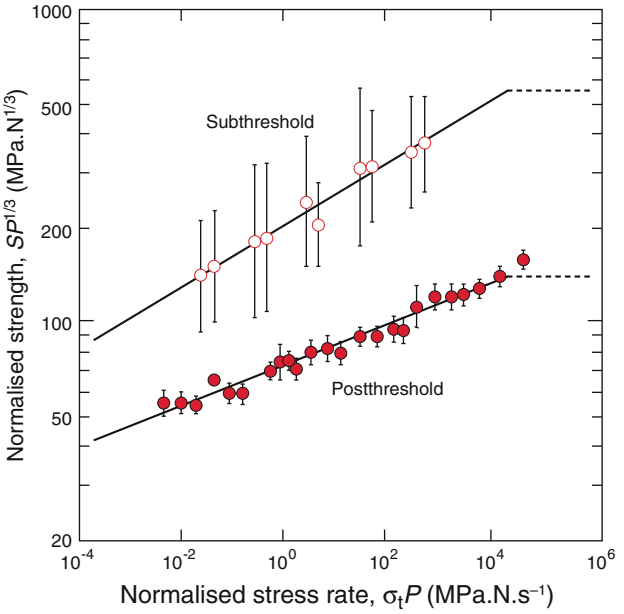

Fig. 18 Load-normalised dynamic fatigue data for soda-lime glass with Vickers postthreshold ($P = 0.5$–10 N) and subthreshold flaws ($P = 150$–250 mN) tested in water. *Dashed lines* are upper-bound strength values for strength tests in inert environment. Data from [113, 114]

Microstructure effects

There is a vast literature on the role of microstructure on mechanical properties of materials. Here we just touch on select examples to illustrate how indentations have been used to investigate this role.

In metals, scaling effects are most clearly demonstrated in the dependence of hardness on grain size l, according to a Hall–Petch relation [116]

$$H = H_0 + k/l^{1/2} \tag{12}$$

with H_0 a macroscopic limit and k a 'Petch parameter'. The l dependence is loosely attributed to reduced stress intensities associated with dislocation pile-ups at the boundaries of smaller grains, making it more difficult to nucleate slip in neighbouring grains. Such hardening with microstructural refinement can transform ordinarily soft metals into a brittle state at ultra-low grain sizes, i.e. in the domain of nanomaterials. However, there is also some suggestion that softening can occur in the nanoscale region. A fundamental understanding of the micromechanisms responsible for the grain size dependence remains a subject of continuing debate, especially in the case of hardness reversal phenomena.

Ceramics are also susceptible to microstructural scaling effects. Fine-grain materials with well-polished surfaces show an analogous Hall–Petch dependence of strength on grain size [117, 118]. Thus the strength of carefully prepared nanocomposite materials increases with diminishing grain size. On the other hand, tests on specimens with controlled indentation flaws demonstrate emphatically (contrary to earlier assertions) that toughness does *not* increase with diminishing grain size [119]. Those tests confirm that the microstructure controls the size of intrinsic flaws. Behavioural changes are also apparent at the opposite end of the microstructural scaling spectrum, in the realm of coarse-grain ceramics and composites. Indentation fracture patterns then tend to be more disjointed and irregular, making it harder to determine toughness from direct crack size measurement [43]. In the coarsest ceramics R–M cracks are suppressed altogether, replaced by a cloud of shear-nucleated microcracks at weak internal interfaces within the confined deformation zone [120]. Such transitions from a brittle to 'quasiplastic' response are most clearly revealed by small sphere indenters, because of the capacity to observe the full evolution of damage from initial elastic contact to full plasticity. An example is shown in Fig. 19 for fine-grain (brittle) and coarse-grain (quasiplastic) micaceous glass–ceramics [120, 121]. In cyclic contact loading, frictional attrition at the intergranular interfaces results in severe mechanical degradation of the contact zone—'contact fatigue' [122–124]. The same intergranular frictional process can effectively increase the toughness of any ensuing R–M cracks, by inhibiting grain pullout across the trailing crack interface [125–127]. Toughness then becomes an increasing function of crack size, so-called R-curve behaviour, with a more pronounced functional dependence in larger grain materials [128]. R-curves can be deconvoluted from indentation–strength data [129], but the domain of heterogeneous structures belongs more firmly in the camp of large-scale engineering testing.

Discussion

The picture of fixed-profile indentation as a universal materials probe evolves from a rich history of mechanical testing extending back well over a century. This article has barely touched on the scope of the subject. We have emphasised the many advantages of indentation testing—its compelling simplicity, its unique capacity for point-to-point sampling and data mapping on a specimen surface, its extraction of materials properties from load and contact dimension measurements, its insight into fundamental underlying deformation and fracture processes, its basis as a model for contact-related processes such as wear and erosion, and its role in providing controlled flaws for quantifying strength properties. We have loosely distinguished between microindentation and nanoindentation: microindentation is especially amenable to materials

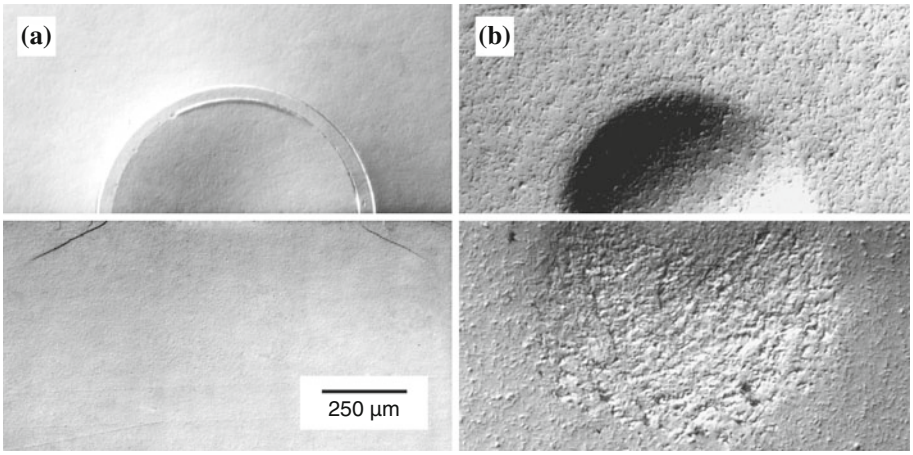

Fig. 19 Contact damage in **a** fine-grain and **b** coarse-grain micaceous glass–ceramic, from indentation with WC sphere of radius 2 mm at load 1000 N, showing a brittle to quasistatic transition. The materials have the same composition in the two cases, and differ only in the heat treatments used to produce the mica crystalline phase. From [121]

testing, requiring only a basic hardness machine along with routine polishing and microscope equipment; nanoindentation is ideal for small-scale specimens and is usually automated but more intricate and requires greater expertise. The main dangers lie in interpretation of the data—of being unaware of the limitations in quantitative evaluation and of regarding the equipment (especially nanoindentation) as a black box.

Perhaps the most widespread use of indentation testing is in the evaluation of material properties, most notably Young's modulus E, hardness H and toughness T. Of these quantities modulus is the most basic, ideally expressible in terms of cohesive force laws but in real materials somewhat dependent on microstructure. It is readily deconvoluted from the unloading portion of the $P(h)$ curve. Discrepancies between values obtained by nanoindentation relative to other, more conventional techniques may arise from uncertainties in evaluation of the machine calibration or other artefacts. Hardness is a more elusive quantity—witness the various empirical attempts over the ages to define it. It depends on indenter geometry—no two indenters give the same value. In well-behaved elastic–plastic materials H provides a measure of yield stress Y, but in other materials it relates more closely to densification or other deformation processes. It is also highly sensitive to compositional variations, and even to trace amounts of impurity (steel). Nevertheless, again because of simplicity in measurement, 'indentation hardness' remains a most resilient measure of resistance to deformation.

Toughness is another ethereal quantity. Whereas in an ideal brittle solid it is expressible in terms of an intrinsic surface energy γ, i.e. $T = (2\gamma E)^{1/2}$, in most materials it involves dissipation of energy over and above that required to create new surfaces [89], dependent on microstructural variables (grain size, porosity, second phase) and environment, as well as on any extraneous fabrication stresses. Consequently, T can vary from batch to batch, specimen to specimen, and even from point-to-point within a single specimen. Given this variability, and mindful of the acknowledged limitations in the fracture equations [47, 48], the indentation method may not be conducive to determination of 'absolute' toughness values. Some argue that the vulnerabilities outweigh the simplicity and advocate discontinuation of indentation as a routine testing protocol altogether [130, 131]. But what is the alternative? Traditional fracture specimens involve exacting fabrication of specimens with machined notches or precracks—an uneconomical and time-consuming process and impractical at small scales. They also require dedicated fracture mechanics expertise and are themselves subject to artefacts and reproducibility issues. Moreover, if indentation toughness is not representative of long-crack values, it follows that long-crack toughness can say little about fracture in the domain of small-scale structures and devices where concentrated stress intensities provide the greatest threat. In any event many behavioural trends, especially those relating to strength in specimens with controlled flaws, can be quantified without recourse to absolute toughness values at all.

Perhaps the greatest asset of indentation testing is the insight it provides into the fundamental processes of deformation and fracture, especially as one heads into the nanoscale domain [11]. It can be made to cover a vast range of indentation sizes and loads (e.g. Figs. 1, 7, 15). It demonstrates how continuum mechanics needs to be replaced by discrete models based on nucleation and initiation events, highlighting the dangers of unconditional downward extrapolation of conventional deformation and fracture laws; there are intrinsic size effects. It enables us to quantify terms like 'brittleness', and accounts for ductile–brittle transitions associated with increasing contact dimension and microstructural refinement. It provides unique information on the ways materials behave under ultra-high stresses, revealing new slip processes and transformation phases. It establishes a generalised framework for determining the micromechanics of the many

different flaw types with or without local residual stress fields, e.g. included particles. It allows for the study of temperature dependence of mechanical properties [132, 133]. Finally, in providing controlled flaws in strength specimens, it enables one to quantify the extreme vulnerability of brittle components to the smallest contacts, even those with no visible cracks.

Indentation technology has a wide diversity of practical applications. Two are illustrated here in Panels—(A) layered structures (coatings and films, composites, interfaces), and (B) biological hard tissues (teeth). Others include the following:

Residual stress evaluation

Residual stresses from materials processing and fabrication can be readily estimated by direct measurement of radial crack lengths or by indentation–strength testing. Tests on stress-free control specimens provide a baseline for evaluation. This approach was first used in thermally tempered and chemically strengthened glasses [134, 135], and has since been applied routinely in a wide range of practical ceramic-based systems. Strategically placed microindentations have also been used to map out the residual elastic–plastic stress fields around larger Vickers indentation sites [136].

Chipping

Chipping near the edge of a brittle structure has long been of concern in the maintenance of engineering structures [137] and the anthropology of stone tool fabrication [138]. Vickers indentations placed close to the edges of glasses and fine-grain ceramics have been used to determine the mechanics of chip formation [139]. Median cracks from the contact site extend stably downward under load to a critical depth before abruptly spalling a chip off the side wall. The equivalent critical load has the form $P/h^{3/2} = \beta T$ (cf. Eq. 5). This relation is cited as another route to toughness evaluation [139].

Cutting, wear and erosion of brittle surfaces

The contact or impact of brittle surfaces with sharp particles can cause strength loss [93, 94] or erosion [42], both of which are readily modelled by indentation theory. At high velocities, particulates may deliver sufficiently intense loads over infinitesimal impact durations as to cause local surface melting in even the most refractory ceramics [140]. A sliding sharp indenter incurs damage along a linear scratch trace [5, 141, 142]: for light (subthreshold) loads, the damage is subthreshold plastic flow; for heavy (postthreshold) loads, heavy microcracking becomes apparent. Cumulative scratching in the subthreshold region is the basis of ultraprecision machining models [143].

Functional materials

The use of indentation, especially nanoindentation, is ideal for probing the properties of small-scale devices such as micro- and nano-electro-mechanical systems (MEMS and NEMS) [144], magnetic storage disks [145], low-k dielectrics [146].

Indentation testing has proved itself to be remarkably durable. It is arguably the most versatile of all mechanical testing techniques. It most assuredly will continue to flourish. For many applications, especially those in the small-scale region, it is the only game in town. At the same time the methodology has its acknowledged limitations—the user should use it wisely, in full knowledge of all its pitfalls as well as its documented advantages.

Panel A: Layered or graded structures—coatings and films, composites, interfaces

There is considerable interest in layered materials structures for functional engineering structures [147]. Coatings or thin films can be applied to protect a vulnerable underlying substrate—by shielding the interior from otherwise deleterious external forces (optical fibres); by providing wear, corrosion or thermal resistance (engine components); by arresting cracks in laminated structures (ceramic armour, shellfish, teeth); by providing electronic function (packaging)—the list goes on. The structures often combine different material types in an effort to extract the best of all worlds. Indentation is particularly useful for characterising layered structures, because of widespread exposure to concentrated contacts during function [148]. We mention only a select few examples here.

An area that has received particular attention is the use of nanoindentation to characterise the deformation of thin films. Analyses taking into account the strong influence of the substrate on the elastic–plastic stress field are available [149–151]. Such analyses can be used to deconvolute E and H values of constituent layer materials. As an illustrative example, Fig. 20 shows raw modulus E and hardness H data plotted as a function of relative indent depth h/d for silicon substrates with oxide and nitride films of thickness d. Asymptotic limits to empirical fits provide values for thin film ($h/d << 1$) and substrate ($h/d >> 1$) materials. Extrapolation to these limits is somewhat subjective, with dependence on the specific $E(h)$ and $H(h)$ relations used.

Indentation is also valuable in elucidating the adhesion properties of brittle films and coatings [152–154]. The

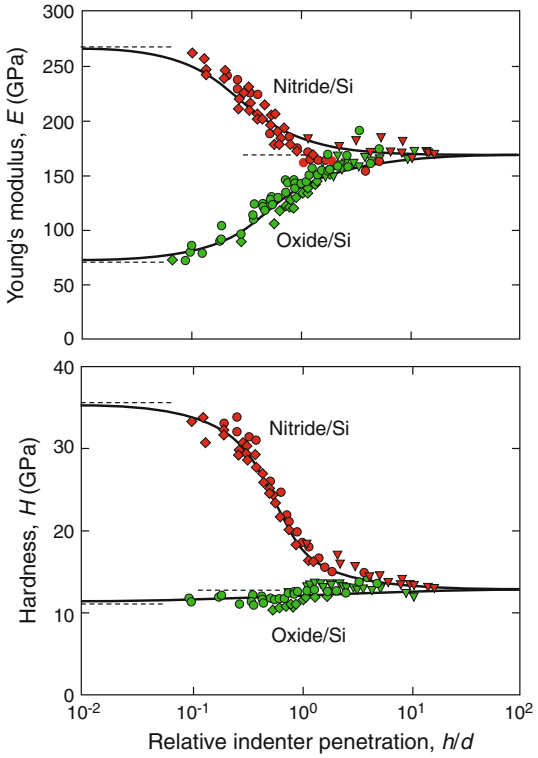

Fig. 20 Plots of nanoindentation modulus E and hardness H as functions of depth-to-thickness h/d. Data are for Si substrates coated with oxide and nitride films. Curves are fits to empirical $E(h)$ and $H(h)$ relations, with asymptotic extrapolations to film (*left*) and substrate (*right*) limits. From [186]

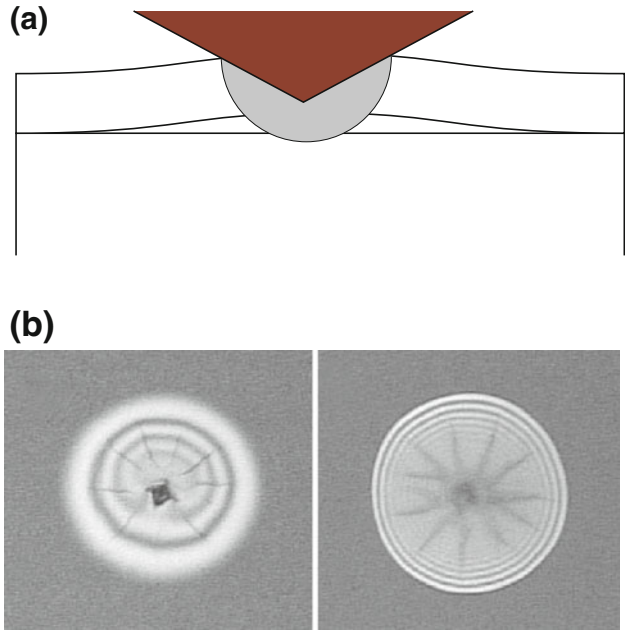

Fig. 21 **a** Schematic depiction of delamination of thin film from substrate at indentation site. **b** Vickers indentation at load $P = 420$ mN in 1.5 μm thick ZnO film on Si substrate. Debonding at interface is visible as fringe pattern, immediately before (*left*) and **b** after (*right*) buckling. From [187]

plastic zone around a sharp indentation drives a lateral crack along a weak film/substrate interface, leading to film delamination. Residual deposition stresses can exacerbate the delamination by causing buckling in the film. The delamination is usually evident as surface uplift around the indentation, enabling measurement of the crack size and calculation of interface toughness. An example is shown in Fig. 21. Film blistering and wrinkling have been observed and analysed in a variety of thin film systems [155–157].

It is possible to study the properties of interfaces in brittle layer systems by placing exploratory microindentations nearby. An example is shown in Fig. 22 for Vickers indentations adjacent to sapphire fibres in a fine-grain alumina matrix [158]. The fibre in (a) is uncoated, that in (b) is coated with a thin layer of monazite ($LaPO_4$). Monazite is uncommonly stable in high-temperature oxidising environments. It also provides a weak interface: whereas in (a) the lead corner crack from the indentation penetrates the interface and passes unhindered into the fibre, in (b) it deflects into the interface and causes debonding. Fibre debonding is an important element of composite toughening, by dissipating energy via frictional pullout behind propagating cracks ('bridging') [126, 159]. Judiciously placed indentations can be used for quantitative evaluation of interface toughness and friction stress [160–162]. An analogous emplacement procedure has been used to quantify the role of interfaces in porcelain veneers fused to zirconia cores for dental crowns [163]. In that case it is functionally desirable that the interface be strong, to prevent catastrophic delamination of the veneer from the core. Variations in the sizes of Vickers radial cracks can be used to quantify any residual stresses in the veneer from interlayer thermal expansion mismatch [164].

Panel B: Biological hard tissues—tooth enamel

Indentation techniques are currently being used in the analysis of hard and soft biological tissues [104, 165]. One example receiving considerable attention is that of tooth enamel, for its relevance to dentistry [166, 167] and evolutionary biology [168–170]. Figure 23 is illustrative, showing Vickers microindentations in (a) a horizontal section through a human molar and (b) a soda-lime glass surface, at a common load. A striking feature of the two patterns is their similarity, despite widely different microstructures: enamel is a little softer and a little tougher than glass, but not by much. Tooth enamel can be modelled as a brittle shell protecting a soft and compliant dentine interior [171, 172].

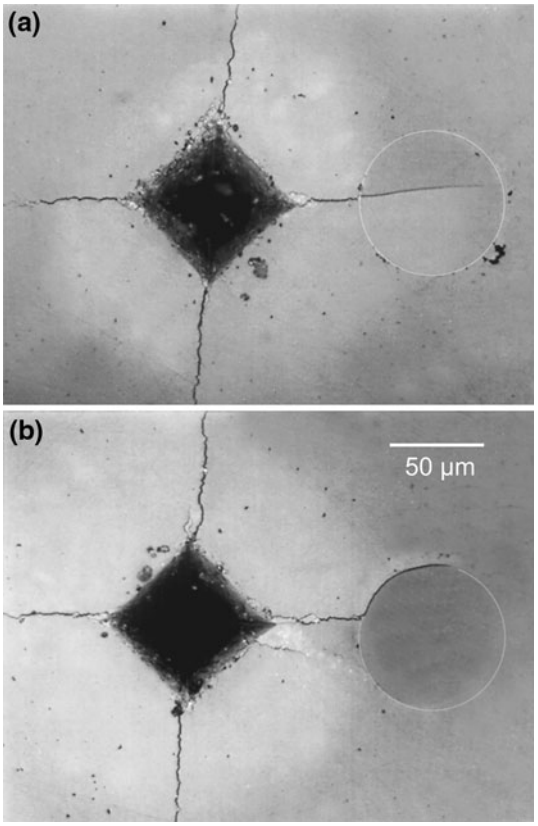

Fig. 22 Vickers indentations placed adjacent to sapphire fibres in a fine-grain alumina matrix: **a** fibre uncoated, showing penetration of corner crack across interface; **b** fibre coated with monazite, showing debonding at weak interface. From [158]

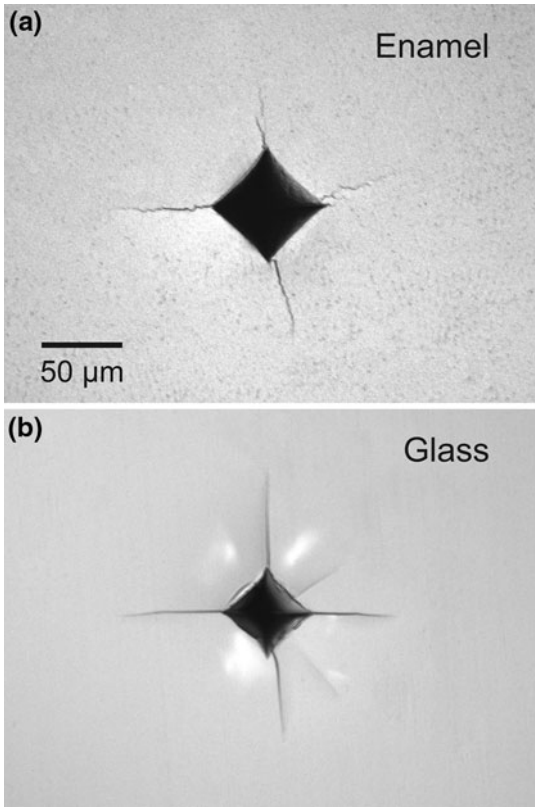

Fig. 23 Vickers indentations in **a** human molar enamel and **b** soda-lime glass, common load $P = 10$ N

We have mentioned the utility of nanoindentation as a means for mapping out mechanical properties across a selected area. In such applications the machine software is programmed to place a closely spaced array of nano-indentations, evaluate modulus E and hardness H at each point, and process the data into a digitised image. Figure 24 is a classic illustration of such mapping across a vertical section through a human molar by Cuy et al. [167]. Significant property gradients are manifest, with stiffer and harder material at the outer surface. One explanation for such gradients is compositional variation from the outer surface to the inner junction between enamel and dentine. Whatever the cause, it is clear that tooth enamel is not a homogeneous structure.

Additional work on property variations has been conducted on the dentition of other primates [173, 174]. Such work is of interest for its implications in the evolutionary process. Nanoindentation data for E and H along linear traces on molar tooth sections of the great apes, including humans, is shown in Fig. 25 [174]. The traces are remarkably similar in all the species, strongly suggestive of a common ancestral past [175].

Tooth enamel has a hierarchical microstructure that can significantly influence mechanical properties. It consists of groups of hydroxyapatite rods weakly bound by fluidized protein sheaths. In a series of papers, He & Swain have applied nanoindentation testing to examine and model the deformation properties of enamel under contact (occlusal-like) loading conditions [176–181]. The weak protein interlayers provide easy slip paths between relatively rigid rods. It is analogous to the push-in of fibres in a reinforced composite [162]. He & Swain envision the deformation taking place by unravelling folded peptide chains within the proteinaceous sheaths. The sheaths are highly susceptible to intrusion of water and exhibit creep. The deformation can recover to some extent, by refolding of the peptide chains. An analogous tendency for recovery is also exhibited at newly formed crack interfaces, by infusion of protein-rich fluids (self-healing) [182].

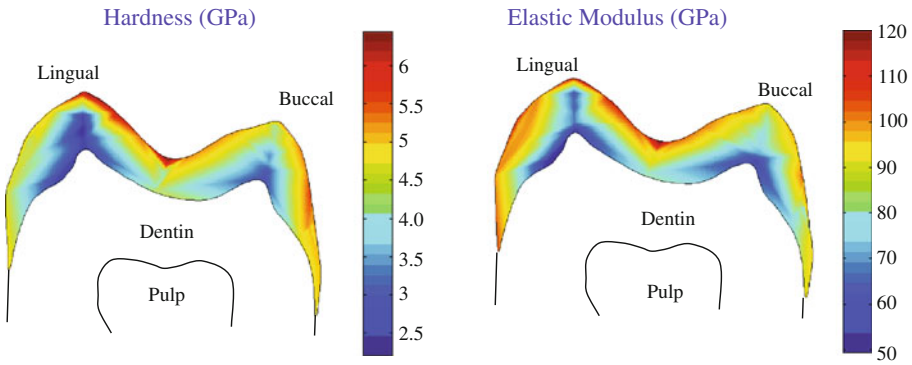

Fig. 24 Hardness and modulus across human molar tooth section. Nanoindentation data map, from Cuy et al. [167]

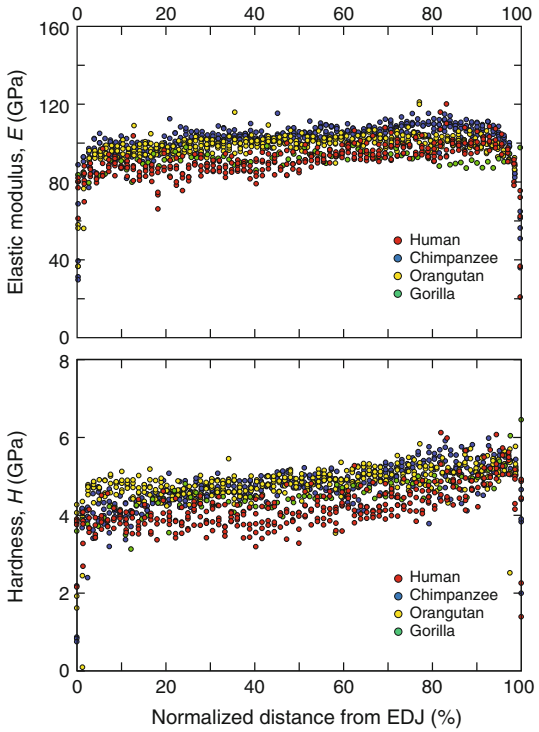

Fig. 25 Profiles of elastic modulus E and hardness H at traces across longitudinal enamel sections in humans and great apes. Normalised section coordinate measured from enamel–dentine junction to outer surface. From [174]

Acknowledgements Gratitude is due to D.B. Marshall, S.M. Wiederhorn and D. Josell for reading the MS and offering valuable suggestions. Countless other colleagues, too many to mention here, have contributed to the work surveyed in this article.

References

1. Hertz H (1896) Hertz's miscellaneous papers. Macmillan, London Chs. 5, 6
2. Tabor D (1951) Hardness of metals. Clarendon, Oxford
3. Samuels LE, Mulhearn TO (1957) J Mech Phys Solids 5:125
4. Johnson KL (1985) Contact mechanics. Cambridge University Press, London
5. Lawn BR, Wilshaw TR (1975) J Mater Sci 10:1049. doi:10.1007/BF00823224
6. Ostojic P, McPherson R (1987) Int J Fract 33:297
7. Cook RF, Pharr GM (1990) J Am Ceram Soc 73:787
8. Johnson K (1982) Proc Inst Mech Eng Tribol 196:363
9. Lawn BR (1998) J Am Ceram Soc 81:1977
10. Hill R (1950) The mathematical theory of plasticity. Oxford University Press, London
11. Lawn BR (2004) J Mater Res 19:22
12. Sneddon IN (1948) Math Proc Camb Philos Soc 44:492
13. Marsh DM (1964) Proc R Soc Lond A282:33
14. Johnson KL (1970) J Mech Phys Solids 18:115
15. Stilwell NA, Tabor D (1961) Proc Phys Soc Lond 78:169
16. Lawn BR, Howes VR (1981) J Mater Sci 16:2745. doi:10.1007/BF02402837
17. Marshall DB, Noma T, Evans AG (1982) J Am Ceram Soc 65:C175
18. Loubet JJ, Georges JM, Meille G (1983) In: Blau PJ, Lawn BR (eds) Micro indentation hardness testing. A.S.T.M. Special Technical Publication 899, Philadelphia, PA, p 72
19. Pharr GM, Cook RF (1990) J Mater Res 5:847
20. Cook RF, Oyen ML (2007) Int J Mater Res 98:370
21. Thurn J, Morris DJ, Cook RF (2002) J Mater Res 17:2679
22. Arora A, Marshall DB, Lawn BR, Swain MV (1979) J Non Cryst Solids 31:415
23. Hagan JT (1979) J Mater Sci 14:462. doi:10.1007/BF00589840
24. Minomura S, Drickamer HG (1962) J Phys Chem Solids 23:451
25. Latella BA, O'Connor BH, Padture NP, Lawn BR (1997) J Am Ceram Soc 80:1027
26. Toivola Y, Stein A, Cook RF (2004) J Mater Res 19:260
27. Zhang J, Wong T-F, Davis DM (1990) J Geophys Res 95:341
28. Oyen ML, Cook RF (2003) J Mater Res 18:139
29. Yoffe E (1982) Philos Mag A 46:617
30. Atkins AG, Silverio A, Tabor D (1966) J Inst Met 94:369
31. Brookes CA, O'Neil JB, Redfern BAW (1971) Proc R Soc Lond 322:73
32. Hockey BJ, Lawn BR (1975) J Mater Sci 10:1275. doi:10.1007/BF00540816
33. Lawn BR, Swain MV (1975) J Mater Sci 10:113. doi:10.1007/BF00541038
34. Evans AG, Wilshaw TR (1976) Acta Metall 24:939
35. Lawn BR, Fuller ER (1975) J Mater Sci 10:2016. doi:10.1007/BF00557479
36. Hagan JT, Swain MV (1978) J Phys D 11:2091
37. Lawn BR, Marshall DB (1984) J Natl Bur Stand 89:435
38. Shetty DK, Wright IG, Mincer PN, Clauer AH (1985) J Mater Sci 20:1873. doi:10.1007/BF00555296

39. Marshall DB, Lawn BR (1979) J Mater Sci 14:2001. doi:10.1007/BF00551043
40. Lawn BR, Evans AG, Marshall DB (1980) J Am Ceram Soc 63:574
41. Marshall DB, Lawn BR, Evans AG (1982) J Am Ceram Soc 65:561
42. Wiederhorn SM, Hockey BJ (1983) J Mater Sci 18:766. doi:10.1007/BF00745575
43. Anstis GR, Chantikul P, Marshall DB, Lawn BR (1981) J Am Ceram Soc 64:533
44. Palmqvist S (1957) Jernkontorets Ann 141:300
45. Nihara K (1983) J Mater Sci Lett 2:221
46. Laugier MT (1985) J Am Ceram Soc 68:C-51
47. Ponton CB, Rawlings RD (1989) Mater Sci Technol 5:865
48. Ponton CB, Rawlings RD (1989) Mater Sci Technol 5:961
49. Evans AG, Charles EA (1976) J Am Ceram Soc 59:371
50. Lawn BR, Jensen T, Arora A (1976) J Mater Sci 11:573. doi:10.1007/BF00540940
51. Lawn BR, Marshall DB (1979) J Am Ceram Soc 62:347
52. Swain MV, Hagan JT (1976) J Phys D Appl Phys 9:2201
53. Hagan JT (1979) J Mater Sci 14:2975. doi:10.1007/BF00611482
54. Hagan JT (1980) J Mater Sci 15:1417. doi:10.1007/BF00752121
55. Lawn BR, Dabbs TP, Fairbanks CJ (1983) J Mater Sci 18:2785. doi:10.1007/BF00547596
56. Lawn BR, Evans AG (1977) J Mater Sci 12:2195. doi:10.1007/BF00552240
57. Fischer-Cripps AC (2002) Nanoindentation. Springer-Verlag, New York
58. Oliver WC, Pharr GM (1992) J Mater Res 7:1564
59. Field JS, Swain MV (1993) J Mater Res 8:297
60. Pharr GM, Harding DS, Oliver WC (1993) In: Nastasi M, Parkin DM, Gleiter H (eds) Mechanical properties and deformation behavior of materials having ultra-fine microstructures. Kluwer Academic Publishers, Dordrecht, p 449
61. Pharr GM (1998) Mater Sci Eng A253:151
62. Morris DJ, Cook RF (2004) J Am Ceram Soc 87:1494
63. Morris DJ, Cook RF (2004) Int J Fract 136:237
64. Morris DJ, Vodnik AM, Cook RF (2004) Int J Fract 136:265
65. Doerner MF, Nix WD (1986) J Mater Res 1:601
66. McColm IJ (1990) Ceramic hardness. Plenum, New York
67. Nix WD, Gao H (1998) J Mech Phys Solids 46:411
68. Ma Q, Clarke DR (1995) J Mater Res 10:853
69. Fleck NA, Muller GM, Ashby MF, Hutchinson JW (1994) Acta Metall Mater 42:475
70. Gane N, Bowden FP (1970) J Appl Phys 39:1432
71. Hill MJ, Rowcliffe DJ (1974) J Mater Sci 9:1569. doi:10.1007/BF00540753
72. Clarke DR, Kroll MC, Kirchner PD, Cook RF, Hockey BJ (1988) Phys Rev Lett 60:2156
73. Page TF, Oliver WC, McHargue CJ (1992) J Mater Res 7:450
74. Stach EA, Freeman T, Minor AM, Owen DK, Cumings J, Wall MA, Chraska T, Hull R, Morris JW, Zettl A (2001) Microsc Microanal 7:507
75. Bradby JG, Williams JS, Wong-Leung J, Swain MV, Munroe P (2001) J Mater Res 16:1500
76. Bradby JG, Williams JS, Wong-Leung J, Kucheyev SO, Swain MV, Munroe P (2002) Philos Mag A 82:1931
77. Zarudi I, Zhang LC, Swain MV (2003) J Mater Res 18:758
78. Piermarini G, Block S (1975) Rev Sci Instrum 46:973
79. Domnich V, Gogotsi Y, Dub S (2000) Appl Phys Lett 76:2214
80. Domnich V, Gogotsi Y (2002) Rev Adv Mater Sci 3:1
81. Jang J, Lance MJ, Wen S, Tsui TY, Pharr GM (2005) Acta Mater 53:1759
82. Gerbig YB, Stranick SJ, Cook RF (2011) Phys Rev B 83:205209
83. Oliver DJ, Bradby JE, Willliams JS, Swain MV, Munroe P (2007) J Appl Phys 101:043524
84. Cottrell AH (1964) The mechanical properties of matter. Wiley, New York
85. Griffith AA (1920) Philos Trans R Soc Lond A221:163
86. Kelly A (1966) Strong solids. Clarendon Press, Oxford
87. Lawn BR (1983) In: Bradt RC, Evans AG, Hasselman DPH, Lange FF (eds) Fracture mechanics of ceramics, vol 5. Plenum, New York, p 1
88. Marshall DB, Lawn BR, Chantikul P (1979) J Mater Sci 14:2225. doi:10.1007/BF00688429
89. Lawn BR (1993) Fracture of brittle solids. Cambridge University Press, Cambridge
90. Lawn BR, Wiederhorn SM, Johnson H (1975) J Am Ceram Soc 58:428
91. Lawn BR, Fuller ER, Wiederhorn SM (1976) J Am Ceram Soc 59:193
92. Lawn BR, Marshall DB (1978) In: Bradt RC, Hasselman DPH, Lange FF (eds) Fracture mechanics of ceramics, vol 3. Plenum, New York, p 205
93. Wiederhorn SM, Lawn BR (1979) J Am Ceram Soc 62:66
94. Wiederhorn SM, Marshall DB, Lawn BR (1979) J Am Ceram Soc 62:71
95. Cook RF, Lawn BR (1983) J Am Ceram Soc 66:C200
96. Jung Y-G, Pajares A, Banerjee R, Lawn BR (2004) Acta Mater 52:3459
97. Dabbs TP, Marshall DB, Lawn BR (1980) J Am Ceram Soc 63:224
98. Dabbs TP, Lawn BR (1985) J Am Ceram Soc 68:563
99. Pajares A, Chumakov M, Lawn BR (2004) J Mater Res 19:657
100. Fairbanks CJ, Polvani RS, Wiederhorn SM, Hockey BJ, Lawn BR (1982) J Mater Sci Lett 1:391
101. Gunasekera SP, Holloway DG (1973) Phys Chem Glasses 14:45
102. Herbert EG, Oliver WC, Lumsdaine A, Pharr GM (2009) J Mater Res 24:626
103. Wright WJ, Nix WD (2009) J Mater Res 24:863
104. Ebenstein DM, Pruitt LA (2006) Nanotoday 1:26
105. Wiederhorn SM, Bolz LH (1970) J Am Ceram Soc 53:543
106. Wiederhorn SM (1974) In: Bradt RC, Lange FF, Hasselman DPH (eds) Fracture mechanics of ceramics. Plenum, New York, p 613
107. Jakus K, Ritter JE, Choi SR, Lardner T, Lawn BR (1988) J Non Cryst Solids 102:82
108. Gupta PK, Jubb NJ (1981) J Am Ceram Soc 64:C112
109. Multhopp H, Lawn BR, Dabbs TP (1984) In: Tressler RE, Bradt RC (eds) Deformation of ceramic materials II. Plenum, New York, p 681
110. Marshall DB, Lawn BR (1980) J Am Ceram Soc 63:532
111. Lawn BR, Marshall DB, Anstis GR, Dabbs TP (1981) J Mater Sci 16:2846. doi:10.1007/BF00552969
112. Fuller ER, Lawn BR, Cook RF (1983) J Am Ceram Soc 66:314
113. Dabbs TP, Lawn BR, Kelly PL (1982) Phys Chem Glasses 23:58
114. Dabbs TP, Lawn BR (1982) Phys Chem Glasses 23:93
115. Cook RF, Lawn BR (1984) In: Freiman SW, Hudson CM (eds) Methods for assessing the structural reliability of brittle materials. A.S.T.M. Special Technical Publication 844, Philadelphia, p 22
116. Petch NJ (1968) In: Liebowitz H (ed) Fracture, vol 1. Academic Press, New York, p Ch. 5
117. Rice RW (1972) Proc British Ceram Soc 20:205
118. Chantikul P, Bennison SJ, Lawn BR (1990) J Am Ceram Soc 73:2419
119. Zhao JH, Stearns LC, Harmer MP, Chan HM, Miller GA, Cook RF (1993) J Am Ceram Soc 76:503
120. Lawn BR, Padture NP, Cai H, Guiberteau F (1994) Science 263:1114
121. Cai H, Stevens Kalceff MA, Lawn BR (1994) J Mater Res 9:762

122. Guiberteau F, Padture NP, Cai H, Lawn BR (1993) Philos Mag A 68:1003
123. Cai H, Kalceff MAS, Hooks BM, Lawn BR, Chyung K (1994) J Mater Res 9:2654
124. Padture NP, Lawn BR (1995) J Am Ceram Soc 78:1431
125. Cook RF, Lawn BR, Fairbanks CJ (1985) J Am Ceram Soc 68:604
126. Swanson PL, Fairbanks CJ, Lawn BR, Mai Y-W, Hockey BJ (1987) J Am Ceram Soc 70:279
127. Mai Y-W, Lawn BR (1987) J Am Ceram Soc 70:289
128. Mai Y-W, Lawn BR (1986) Ann Rev Mater Sci 16:415
129. Braun LM, Bennison SJ, Lawn BR (1992) J Am Ceram Soc 75:3049
130. Quinn GD, Bradt RC (2007) J Am Ceram Soc 90:673
131. Kruzic JJ, Kim DK, Koester KJ, Ritchie RO (2009) J Mech Behav Biomed Mater 2:384
132. Atkins AG, Tabor D (1966) Proc R Soc Lond A292:441
133. Naylor NGF, Page TF (1983) J Microsci 130:345
134. Marshall DB, Lawn BR (1977) J Am Ceram Soc 60:86
135. Chantikul P, Lawn BR, Marshall DB, Drexhage MG (1979) J Am Ceram Soc 62:551
136. Zeng K, Rowcliffe DJ (1995) Acta Metall 43:1935
137. Almond EA, McCormick NJ (1986) Nature 321:53
138. Cotterell B, Kaminga J, Dickson FP (1985) Int J Fract 29:205
139. Chai H, Lawn BR (2007) Acta Mater 55:2555
140. Lawn BR, Hockey BJ, Wiederhorn SM (1980) J Am Ceram Soc 63:356
141. Swain MV (1980) Glass Technol 21:290
142. Cook RF (1994) J Am Ceram Soc 77:1263
143. Blake PN, Scattergood RO (1990) J Am Ceram Soc 73:949
144. Ballarini R, Mullen RL, Yin Y, Kahn H, Stemmer S, Heuer AH (1997) J Mater Res 12:915
145. Bushan B (1990) Tribology and mechanics of magnetic storage devices. Springer-Verlag, New York
146. Morris DJ, Cook RF (2008) J Mater Res 23:2429
147. Freund LB, Suresh S (2004) Thin film materials: stress, defect formation and surface evolution. Cambridge University Press, Cambridge
148. Lawn BR, Deng Y, Miranda P, Pajares A, Chai H, Kim DK (2002) J Mater Res 17:3019
149. Bhattacharya AK, Nix WD (1988) Int J Solids Struct 24:1287
150. Gao H, Chiu C-H, Lee J (1992) Int J Solids Struct 29:2471
151. Xu H, Pharr GM (2006) Scr Mater 55:315
152. Marshall DB, Evans AG (1984) J Appl Phys 56:2632
153. Rossington C, Marshall DB, Evans AG, Khuriyakub BT (1984) J Appl Phys 56:2639
154. Cordill MJ, Bahr DF, Moody NR, Gerberich WW (2004) Dev Mater Reliab 4:163
155. Bowden N, Brittain S, Evans AG, Hutchinson JW, Whitesides GM (1998) Nature 393:146
156. Thurn J, Cook RF (2004) J Mater Sci 38:4799. doi:10.1023/B:JMSC.0000035318.95497.d1
157. Thurn J, Cook RF (2004) J Mater Sci 38:4809. doi:10.1023/B:JMSC.0000035319.81486.62
158. Morgan PED, Marshall DB (1995) J Am Ceram Soc 78:1553
159. Marshall DB, Cox BN, Evans AG (1985) Acta Metall 23:2013
160. Marshall DB (1984) J Am Ceram Soc 67:C259
161. Becher PF, Sun EY, Hseuh CH, Alexander KB, Waters SL, Westmoreland CG (1996) Acta Mater 44:3881
162. Marshall DB, Morgan PED, Housley RM (1997) J Am Ceram Soc 80:1677
163. Kim J-W, Bhowmick S, Hermann I, Lawn BR (2006) J Biomed Mater Res 79B:58
164. Hermann I, Bhowmick S, Zhang Y, Lawn BR (2006) J Mater Res 21:512
165. Oyen ML (2011) Handbook of nanoindentation with biological applications. Pan Stanford, Singapore, p 1
166. Xu HHK, Smith DT, Jahanmir S, Romberg E, Kelly JR, Thompson VP (1998) J Dent Res 77:472
167. Cuy JL, Mann AB, Livi KJ, Teaford MF, Weihs TP (2002) Arch Oral Biol 7:281
168. Lucas PW (2004) Dental functional morphology: how teeth work. Cambridge University Press, Cambridge
169. Lucas PW, Constantino PJ, Wood BA, Lawn BR (2008) BioEssays 30:374
170. Ungar PS (2010) Mammal teeth. Johns Hopkins University Press, Baltimore
171. Chai H, Lee JJ-W, Constantino PJ, Lucas PW, Lawn BR (2009) Proc Natl Acad Sci USA 106:7289
172. Lee JJ-W, Constantino PJ, Lucas PW, Lawn BR (2011) Biol Rev. doi:10.1111/j.1469-185X.2011.00181.x
173. Darnell LA, Teaford MF, Livi KJT, Weihs TP (2010) Am J Phys Anthropol 141:7
174. Lee JJ-W, Morris D, Constantino PJ, Smith TM, Lawn BR (2010) Acta Biomater 6:4560
175. Constantino PJ, Lee JJ-W, Grbig Y, Hartstone-Rose A, Talebi M, Lawn BR, Lucas PW (in press) Am J Phys Anthropol
176. He LH, Fujisawa N, Swain MV (2006) Biomaterials 27:4388
177. He LH, Swain MV (2007) Appl Phys Lett 90(171916):171911
178. He LH, Swain MV (2007) J Dent 35:431
179. He LH, Swain MV (2007) Biomaterials 28:4512
180. He LH, Swain MV (2007) Dent Mater 23:814
181. Xie Z-H, Swain MV, Swadener G, Munro P, Hoffmann M (2009) J Biomech 42:1075
182. Myoung S, Lee JJ-W, Constantino PJ, Lucas PW, Chai H, Lawn BR (2009) J Biomech 42:1947
183. Cook RF, Liniger EG, Steinbrech RW, Deuerler F (1994) J Am Ceram Soc 77:303
184. Oliver DJ, Lawn BR, Cook RF, Reitsma MG, Bradby JE, Williams JS, Munroe P (2008) J Mater Res 23:297
185. Lawn BR, Jakus K, Gonzalez AC (1985) J Am Ceram Soc 68:25
186. Jung Y-G, Lawn BR, Martyniuk M, Huang H, Hu X (2004) J Mater Res 19:3076
187. Huang B, Zhao M-H, Zhang T-Y (2004) Philos Mag 84:1233